2

Low-Frequency Response and the Skin-Electrode Interface in Dry-Electrode Electrocardiography

Cédric Assambo and Martin J. Burke
University of Dublin, Trinity College
Ireland

1. Introduction

In recent years, there has been a growing interest in the area of ambulatory electrocardiogram (ECG) recording using dry or unjelled electrodes for long-term physiological monitoring. The key advantage of dry electrodes is the elimination of allergic reactions or other forms of skin irritation, commonly associated with electrolyte gels. It results in the improvement of patient comfort and compliance, allowing the recording technique to cater for a wider range of users such as elderly, the long-term ill, cardiac rehabilitation patients, paediatrics and neonates. Furthermore, dry-electrode recording does not require preparation of the electrodes before or after application apart from cleaning and they can be re-used almost indefinitely. The durability of dry electrodes over gel-based ones permits their shelf-life to be extended and considerably increases the length of time for which they can be worn, allowing long-term ambulatory ECG recording at much lower cost. Embedded in remote telemetry systems, dry-electrode ECG recording can thus contribute to the improvement of health care delivery.
The investigation of the use of dry electrodes for ECG monitoring has led to the development of several pasteless electrode systems which overcome the disadvantages associated with traditional approaches employing wet electrodes. The following question however was immediately raised: how should the recording amplifier be adapted to the high source impedance commonly associated with dry electrodes? Optimised designs of the amplifier front-end have usually involved measuring the impedance of the skin-electrode interface (Burke & Gleeson, 2000; Chang et al., 2010; Ko et al., 1970; Mühlsteff & Such, 2004; Valverde et al., 2004). Some solutions have then inserted resistors in series with unbalanced electrodes to match the effective impedance seen at each input of the recording amplifier (Lee et al., 2006). Others have fabricated dry electrodes having impedances lower in magnitude than those of conventional Ag/AgCl wet electrodes (Chang et al., 2010; Wolfe & Reinhold, 1974). Commercial dry-electrode Holter monitors providing diagnostic quality ECGs are however not available to date. The recent development in 2009 of a wearable two-channel dry-electrode ECG system called *care.mon* has shown some prospects in the realisation of long-term telemetric application in the near future (Fuhrhop et al., 2009). The designers have admitted, however, that their prototype cannot get a signal of the same quality as that of a standard electrode Holter system.
A critical source of error was soon identified as low-frequency distortion introduced at the amplifier's front-end. In this chapter, the authors show how high-pass filtering can affect the quality of the recorded ECG waveform and demonstrate that the risk of distortion is

exacerbated by the presence of a frequency dependent skin-electrode impedance. New approaches for the determination of the model parameters of the skin-electrode interface and new input impedance requirements for dry-electrode ECG recording are then presented.

2. Importance of the recorder's low-frequency response in diagnostic quality electrocardiography

To ensure that the electrocardiograph's output signal is an accurate representation of the physiological input waveform, the amplifier must faithfully reproduce all frequency components of the ECG signal. Out-of-band high frequency interfering signals are normally removed from the preamplifier's output by implementing linear-phase low-pass filters. However, distortion introduced by an inadequate low-frequency response cannot generally be corrected in real time by simple filtering in the subsequent amplification stages (Tayler & Vincent, 1983). The quality of the recorder's low-frequency response relies therefore on the performance of the preamplifier's front-end. To prevent recording error caused by the electrocardiograph, the preamplifier must preserve the ECG signal by providing flat amplitude response and linear or zero phase within the ECG bandwidth (Berson & Pipberger, 1966; Tayler & Vincent, 1983). Failure to fulfil these requirements can have serious clinical implications.

2.1 Diagnostic implications of a poor low-frequency response

Berson & Pipberger have demonstrated that ECG preamplifiers implementing high-pass filters with a poor low-frequency amplitude response are a potential source of recording error that may lead to misdiagnosis of serious cardiac conditions (Berson & Pipberger, 1966). They concluded that an increase of the filter's cutoff frequency above 0.05 Hz or a roll-off greater than 6 dB per octave causes distortion of the S-T segment and the T wave of the ECG waveform. Yet, accurate measurement of slow deflections, especially in the first quarter of the ST-T complex, is usually crucial for assessing the condition of the heart and its response to therapy (Symanski & Gettes, 1993). For example, acute myocardial infarction, commonly known as heart attack, is frequently accompanied by an elevation of the ST segment but inadequate low-frequency response reduces this elevation and can produce an inversion of the terminal part of the T wave, as shown in Fig. 1(a). In addition, it was reported that the ECG of patients who had suffered damage to the surface of the heart, referred to as an old infarct, usually shows a downward sloping S-T segment (Berson & Pipberger, 1966). Fig. 1(b) illustrates how poor high-pass filtering can modify the S-T segment by converting a downward slope into an upward slope, which has a different clinical interpretation.

It was found that low-frequency distortion is generally greater for abnormal than for normal ECG waveforms and for records having essentially monophasic QRS patterns than for those having biphasic QRS complexes. Besides, it was observed that the increase in heart rate associated with exercise can alter recording error in an unpredictable manner (Berson & Pipberger, 1966).

The works of Berson & Pipberger were followed by studies led by Tayler & Vincent on the low-frequency phase response of filters used in ECG recording (Tayler & Vincent, 1983). They concluded that phase nonlinearity is also a major source of recording error and misdiagnosis. For example, myocardial ischaemia is a disease that reduces the supply of blood to the heart muscle and normally manifests itself in the ECG record as elevation or depression of ST segments (Lynch et al., 1980). However, false ST segment shifts such as those depicted in Fig. 2(a) have been noted with ambulatory ECG recorders exhibiting a nonlinear phase

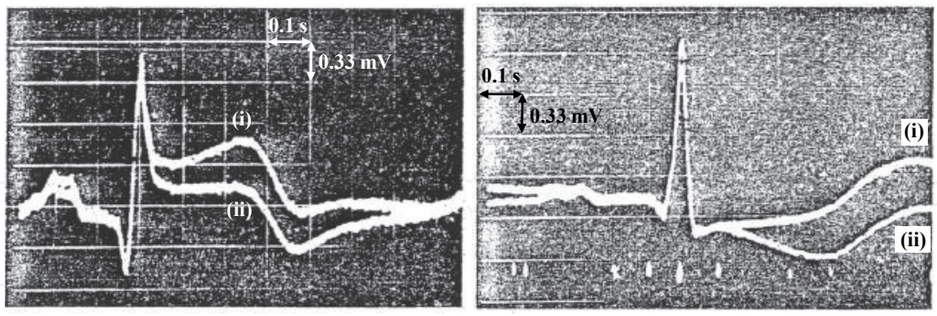

(a) Acute infarct record. (b) Old infarct record.

Fig. 1. Oscilloscope photographs of the electrocardiogram of patients suffering from (a) acute myocardial infarction and (b) an old infarct (from (Berson & Pipberger, 1966)). In both pictures, the upper record, labelled (i), is obtained with a simulated dc amplifier system while the lower record , (ii), is the output of a high-pass filter having a 0.5-Hz cutoff and 24-dB-per-octave roll-off.

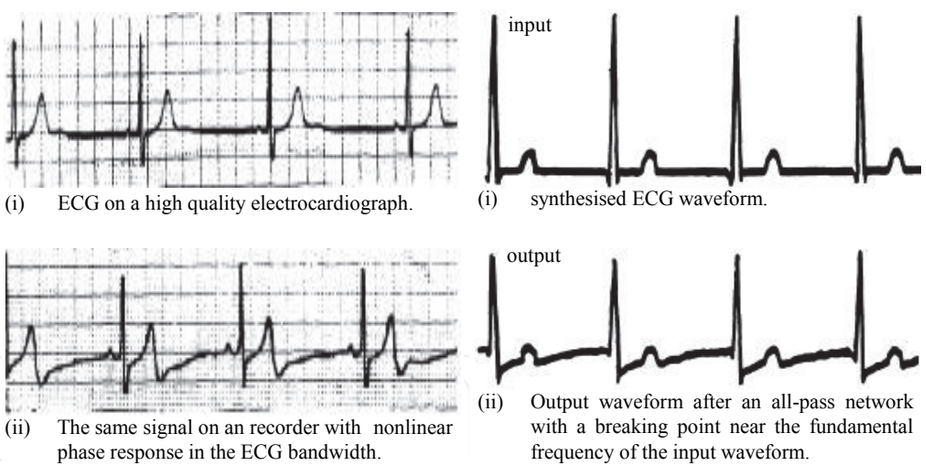

(i) ECG on a high quality electrocardiograph.

(i) synthesised ECG waveform.

(ii) The same signal on an recorder with nonlinear phase response in the ECG bandwidth.

(ii) Output waveform after an all-pass network with a breaking point near the fundamental frequency of the input waveform.

(a) Effect of phase distortion on a patient's ECG.

(b) Effect of an all-pass network with nonlinear phase response.

Fig. 2. Electrocardiograms showing the effect of low-frequency distortion caused by nonlinear phase response in the bandwidth of the ECG signal from (a) a patient's record and (b) a synthesised ECG waveform (modified from (Tayler & Vincent, 1983)). In (b), the input waveform is filtered by an all-pass network with flat amplitude response from dc to 10 kHz ($\pm$ 1 dB), but a nonlinear phase response with a breaking point approaching the fundamental frequency of the input waveform.

response at low frequency. Results revealed that the ST segment is more readily affected by distortion when the point of maximum phase nonlinearity approaches the fundamental frequency of the ECG signal, as shown in Fig. 2(b). Once phase nonlinearity is introduced at the preamplifier front stage, its effects on the ST-T complex cannot be corrected subsequently without distorting other portions of the ECG waveform (Tayler & Vincent, 1983).

2.2 Low-frequency performance requirements of ECG recorders

The empirical findings reported in (Berson & Pipberger, 1966) and (Tayler & Vincent, 1983) have played a key role in defining the frequency response requirements of ECG recorders utilised today and can be considered as part of the classical publications in ECG signal conditioning. The traditional performance criteria have been enhanced by the addition of specifications in the time domain. The evolution of the low-frequency performance requirements in electrocardiography can be summarised as follows:

1. In the mid 1960s, to ensure that recording errors are kept under 50 μV in the early portion of the ST-T complex, Berson & Pipberger recommended that ECG preamplifiers provide a 0.05-Hz low-frequency cutoff with a 6-dB-per-octave roll-off (Berson & Pipberger, 1966), as achieved for example by a single-pole high-pass filter. The American Heart Association (AHA) has endorsed this low-frequency cutoff since 1967 (A.H.A., 1967) and added in 1985 that the amplitude response should be flat to within ±6 % (0.5 dB) over the range 0.14 to 30 Hz (A.H.A., 1985), as shown in Fig. 3(a).
2. In the early 1980s, Tayler & Vincent recommended that phase linearity must be maintained down to the fundamental frequency of the physiological signal to allow high fidelity in the reproduction of the ECG waveform (Tayler & Vincent, 1983). The AHA has adopted this recommendation since 1985 by specifying that the phase shift introduced by the amplifier should not be greater than that introduced by a 0.05-Hz, single-pole high-pass filter (A.H.A., 1985), as depicted in Fig. 3(b).
3. In more recent years, specification of the low-frequency performance of electrocardiographs based on the system's impulse response have been introduced. The International Electrotechnical Committee (IEC) and the American National Standard Institute (ANSI) have indicated that a 300-μVs impulse shall not yield an undershoot on the ECG record from the isoelectric line of greater than 100 μV, and shall not produce a recovery slope of greater than 300 μVs^{-1} following the end of the impulse (Berson et al., 2007; I.E.C., 2001), as illustrated in Fig. 4.

2.3 The effect of high-pass filtering on the ECG signal

The performance requirements can be explained from a simple mathematical model of the physiological signal and the recording system. From a signal viewpoint, the ECG waveform may be regarded as a periodic time function represented by the following Fourier series:

$$f(t) = \sum_{n=0}^{\infty} \left[\alpha_n cos\left(\frac{2\pi nt}{T_{R-R}}\right) + \beta_n sin\left(\frac{2\pi nt}{T_{R-R}}\right) \right] \quad (1)$$

where T_{R-R} is the $R-R$ interval or cardiac cycle time and α_n and β_n are the Fourier coefficients. The fundamental frequency of the ECG signal is therefore determined by $1/T_{R-R}$ and defines the heart rate while its dc component is given by α_0.

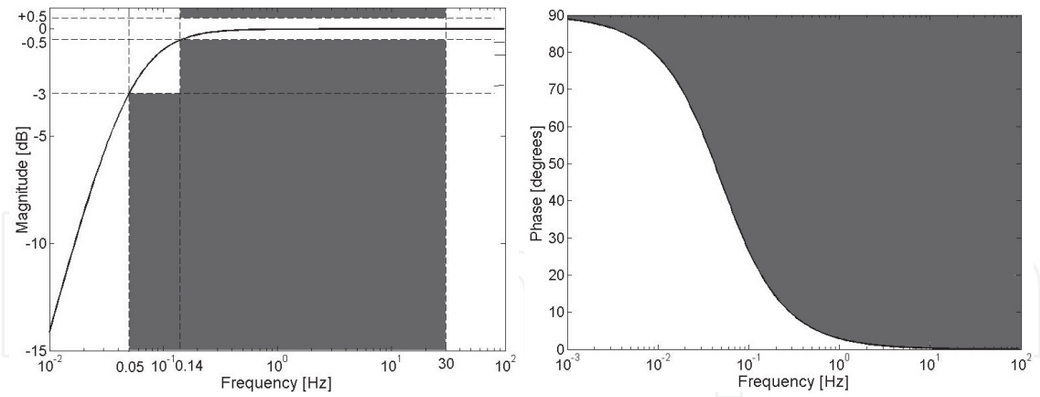

(a) Amplitude response criterion (b) Phase response criterion

Fig. 3. Plots of the low-frequency (a) amplitude and (b) phase criteria illustrated with a 0.05-Hz single-pole high-pass filter. The shaded areas indicate the "forbidden" areas as specified by the AHA (A.H.A., 1985).

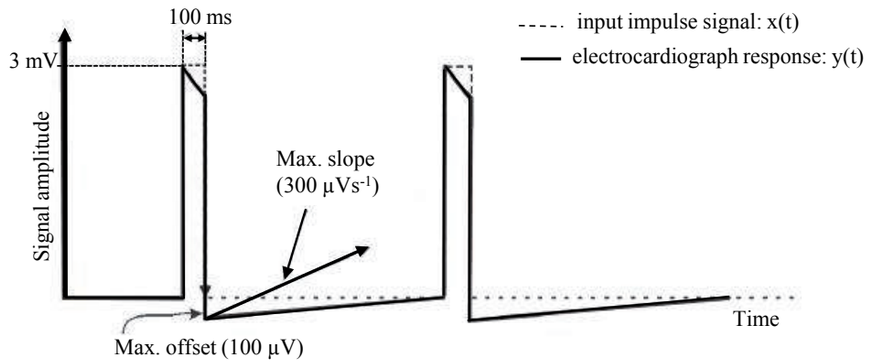

Fig. 4. Plots of the impulse response requirements (from (Berson et al., 2007; I.E.C., 2001)).

If $A(s)$ represents the preamplifier's transfer function, its response to the ECG signal defined in eq. (1) can then be modelled in the Laplace domain by the following product:

$$V_{out}(s) = A(s) \int_0^\infty f(t) e^{-st}\, dt \tag{2}$$

$V_{out}(t)$, the preamplifier's response to $f(t)$ in the time domain, is obtained from the inverse Laplace transform of eq. (2) by convolution once $A(s)$ is known.
Taking $s = j\omega$, the preamplifier response may also be specified in the frequency domain as follows:

$$A(j\omega) = |G(\omega)|\, e^{j\theta(\omega)} \tag{3}$$

with $|G(\omega)|$ its amplitude response and $\theta(\omega)$ its phase response. An ideal amplitude response is achieved when $|G(\omega)|$ is frequency-independent, which in practice would require the ECG recorder to be dc-coupled to the source signal. This approach is, however, inadvisable due to excessive base-line wander and artefacts commonly associated with dc-coupled recording equipment. In addition, the large dc offset inherently present with dry electrodes would quickly limit the obtainable gain of the amplification stages due to saturation. AC-coupling is

therefore unavoidable in diagnostic quality ECG recording but it comes at the cost of potential amplitude and phase distortion as outlined by (Berson & Pipberger, 1966) and (Tayler & Vincent, 1983). Because of phase nonlinearity, a non-constant group delay is introduced into the ECG waveform. Consequently the low-frequency components of the QRS complex are affected by a greater time delay than its high-frequency components and can therefore become superimposed on the ST complex (Tayler & Vincent, 1983). Low-frequency phase distortion is avoided if the phase shift or the group delay is made negligible. For example, the phase shift introduced by a first order high-pass filter is less than 6° from a decade above the cutoff frequency, f_c. Therefore, if frequencies in the vicinity of the fundamental ECG frequency are to be reproduced, the 3-dB low-frequency point must be about 10 times lower than $1/T_{R-R}$. Considering a lower limit heart rate of 30 beats per minute gives $1/T_{R-R} = 0.5$ Hz and thus $f_c = 0.05$ Hz.

The impulse response requirements complement the frequency response specifications to ensure that the fast varying signals in the ECG, such as the QRS complex and P wave, do not generate noticeable depressions as result of filtering. A visible undershoot could, in fact, be misinterpreted as an additional ECG component. The Common Standards for Quantitative Electrocardiography (CSE) issued by the European Union defines the presence of a QRS deflection as a waveform having an amplitude greater than or equal to 20 μV and a duration greater than or equal to 6 ms (Berson et al., 2007). Moreover, the slope of the response after the end of the input impulse must be minimised to preserve base line stability and allow accurate amplitude measurement of the P wave and the QRS complex.

3. Effect of the skin-electrode interface on the low-frequency performance of ECG recording systems

High pass-filtering is commonly achieved in dry-electrode ECG recording by inserting a dc-blocking capacitor, C_{in}, in series with each sensing electrode as shown in Fig. 5. Z_s simulates the skin-electrode impedance and R_{in} is the input impedance of the recording amplifier. Two electrical models of have been principal used to simulate the skin-electrode interface at the preamplifier's input: a simple single-time-constant RC network and a more complete double-time-constant model.

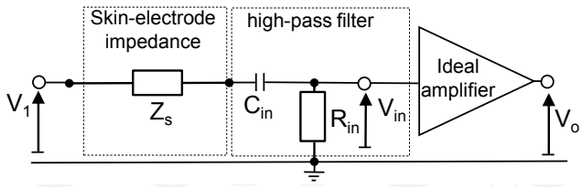

Fig. 5. Schematic representation of a simple high-pass filter at the amplifier's front-end. AC-coupling achieved this way allows dc offset voltages associated with polarisation effects at the skin-electrode interface to be blocked from the amplifier input.

3.1 A single-time-constant model of the skin-electrode interface

Fig. 6 shows the general form of the single-time-constant skin-electrode model which represents the impedance of the electrode with a resistor, R_e, in parallel with a capacitor, C_e, while the lumped resistance of the skin and body tissue is simulated by a resistor, R_s. However, because of its relatively low value, R_s is often omitted. The electrode polarisation potential is modelled with a dc voltage source, V_{DC}.

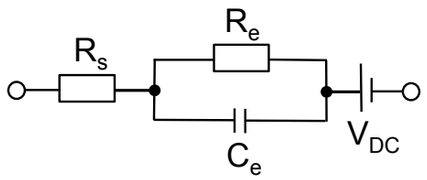

Fig. 6. A standard single-time-constant representation of the skin-electrode interface. The half-cell potential, V_{DC}, introduces a dc offset but does not contribute to the ac impedance of the interface.

The parameter values stipulated in international standards issued by both IEC and ANSI are R_e =0.62 MΩ and C_e=4.7 nF (Berson et al., 2007; Bruce et al., 2007; I.E.C., 2001; 2005). In all standards it is stated that the skin-electrode impedance in series with any patient-electrode connection must not result in a signal reduction of more than 6% of that obtained without the simulated impedance. The standards specify that the preamplifier must provide an input impedance of at least 10 MΩ at 10 Hz, since the magnitude of the simulated source impedance would be equal to 0.6 MΩ at this frequency. In addition, a low-frequency cutoff at 0.05 Hz or lower must be achieved by the amplifier, with the simulated skin-electrode impedance disconnected. Given R_{in} = 10 MΩ, an input capacitance C_{in} = 0.33 μF is required to implement a 0.05-Hz single-pole high-pass filter at the amplifier input. It must be noted, however, that the input impedance specification does not take into account phase response, impulse response or attenuation below 10 Hz.

In 2004, considering the amplitude and phase criteria recommended by the AHA (A.H.A., 1990), the relationship between input impedance requirement and source impedance was analytically studied by Valverde et al (Valverde et al., 2004) who suggested that for frequencies below 100 Hz, the interface can be approximated by the electrode resistance, R_e. It was concluded that an amplifier having a low-frequency input impedance $R_{in} > 17R_e$ would not cause more than 6% attenuation at 0.14 Hz nor introduce a phase shift of greater than 6° at 0.5 Hz. Based on electrode resistance R_e = 150 kΩ, R_{in} was estimated at 2.4 MΩ at 0.14 Hz and the dc-blocking capacitor was chosen as C_{in} = 2.2 μF.

In 2000, Burke & Gleeson (Burke & Gleeson, 2000) estimated the component values of the skin-electrode interface as R_s = 10 kΩ, R_e = 1.4 MΩ and C_e= 20 nF. The preamplifier front-end was designed so that its input impedance would be significantly larger than that of the skin-electrode impedance to minimise interference caused by motion artefact and unwanted common-mode voltages. It was reported that the attenuation caused by R_s is limited to 1% for $R_{in} > 100R_s$ and the phase shift introduced by R_e and C_e is kept below 1° in the bandwidth of the ECG signal for $R_{in} > 60R_e$. The designed low-power preamplifier achieved an input impedance of 260 MΩ and was coupled with a 1 μF dc-blocking capacitor.

Emphasis must be placed on the fact that input impedance requirements have not traditionally included impulse response criteria. The authors have therefore evaluated the performance of simulated high-pass filters based on the models outlined above to assess whether or not amplitude, phase and impulse response criteria would be simultaneously met when the electrode impedance is taken into account. A program was written in *MATLAB* to determine and plot the low-frequency response of the skin-electrode-amplifier networks based on the provided skin-electrode model and the amplifier's front-end design. Plots of the simulated amplitude, phase and impulse responses, together with the recovery slope are shown in Fig. 7. Results are compared with the response of a 0.05-Hz single-pole high-pass

filter equivalent to the amplifier operating with a dc-blocking capacitor but omitting the skin-electrode impedance. A summary is given in Table 1.

	max. magitude 0.14-30 Hz [dB]	phase @ 0.5 Hz [°]	max. undershoot after impulse [mV]	max. slope [mVs^{-1}]
specification limit	-0.5	6	-0.1	0.3
0.5-Hz single-pole high-pass filter	-0.5	5.8	-0.093	0.03
IEC min. input impedance requirement	**−0.96**	5.3	**−0.25**	**53.6**
solution proposed by Valverde et al	-0.5	4.1	**−0.11**	**0.49**
solution proposed by Burke & Gleeson	-0.05	0.1	-0.02	**0.55**

Table 1. Low-frequency performance of simulated skin-electrode-amplifier networks compared to that of a single-pole 0.05-Hz high-pass filter. Bold case indicates that performance requirement is not met.

Columns 2 and 3 indicate the maximum attenuation in the frequency range 0.14 to 30 Hz and the phase shift at 0.5 Hz, respectively. Plots of the frequency response are presented in Figs. 7(a) and 7(b), which suggest that the amplitude and phase criteria would not be met if the IEC minimum input impedance requirement was applied with the electrodes used in international standards. It can be observed that the capacitive component of the simulated skin-electrode introduces additional phase shift into the signal for frequencies above 10 Hz. However, these criteria are fulfilled in the case of designs suggested by Valverde et al. and Burke & Gleeson.
Plots of the time response of the systems to a 300-mVs input impulse are presented in Fig. 7(c). The fourth column of Table 1 gives the maximum value of the undershoot following the input impulse. It can be seen that the simulated impulse response using the minimum input impedance specified by the IEC or Valverde's solution would result in undershoots greater than the specified limit. The threshold is however respected for the simulated system based on the design proposed by Burke & Gleeson. Fig. 7(d) shows the corresponding recovery slope and the last column of Table 1 gives its maximum value that must be limited in magnitude to 0.3 mVs^{-1} to meet requirements. Results indicate that all three simulated skin-electrode-amplifier networks would exceed the specified maximum recovery slope. The recovery slope is significantly high when the IEC minimum input impedance requirement is followed since it is expected to reach a maximum of 55.6 mVs^{-1}, about 185 times the specification limit.
These results demonstrate that amplitude, phase and impulse response criteria are not met if the minimum IEC input impedance requirement is applied. In addition, an unsatisfactory recovery slope is exhibited by electrocardiographs despite following the amplitude and phase recommendations. The results also demonstrate that the risk of signal distortion can only be assessed with accuracy when the skin-electrode impedance is taken into account.

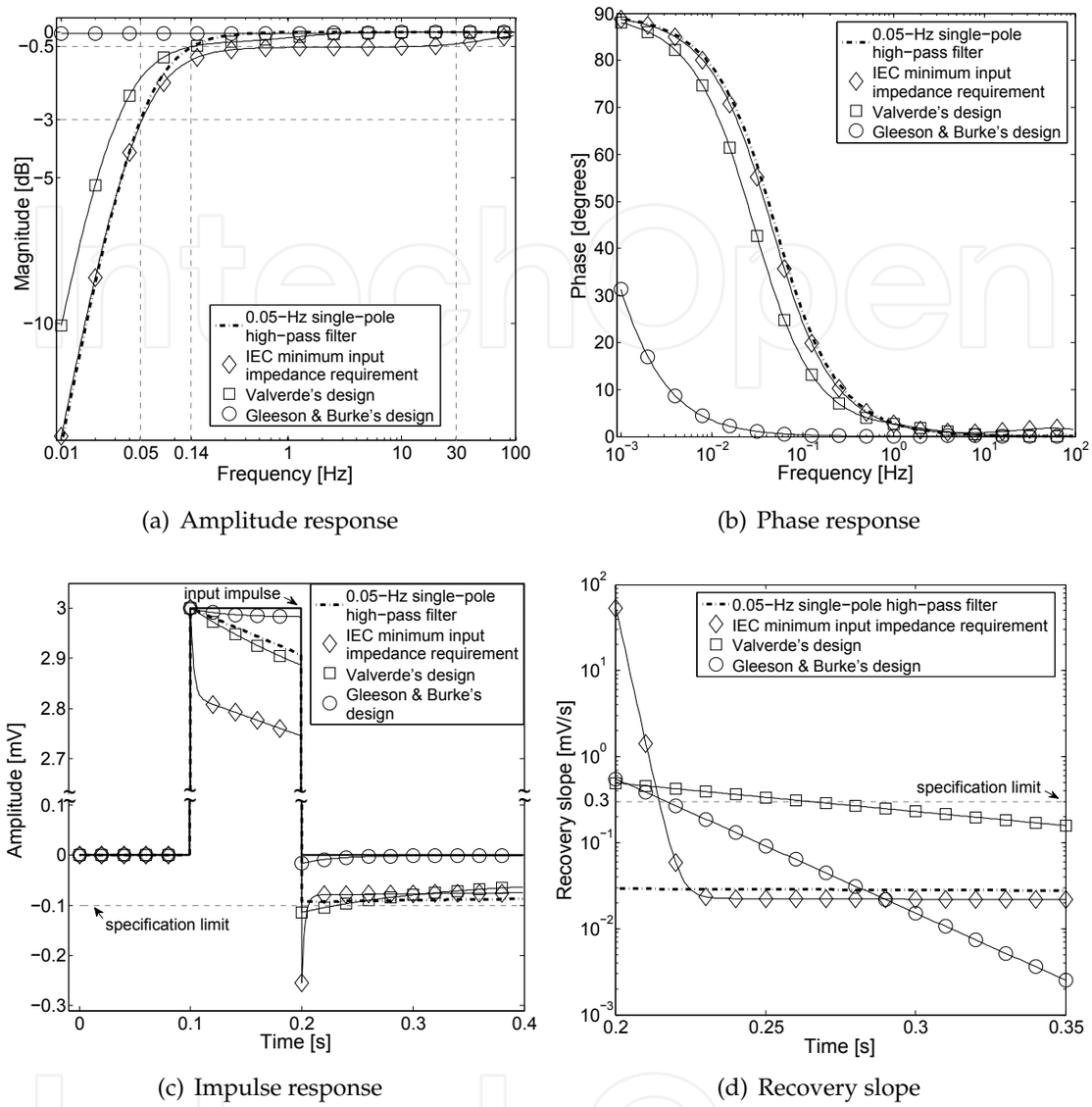

(a) Amplitude response

(b) Phase response

(c) Impulse response

(d) Recovery slope

Fig. 7. Plots of (a) the amplitude response, (b) phase response, (c) impulse response and (d) recovery slope of the simulated skin-electrode-amplifier networks compared to that of a single-pole 0.05-Hz high-pass filter.

3.2 A double-time-constant model of the skin-electrode interface

Using the double-time-constant model depicted in Fig. 8(a), Mühlsteff et al. investigated in 2004 the complex impedance of the skin-electrode interface of silicone rubber dry electrodes (Mühlsteff & Such, 2004). Measurements, taken in the frequency range 0.1 to 1000 Hz indicated that the ac behaviour of the skin-electrode contact interface is not accurately simulated by a single parallel RC-model. They proposed a double RC model with parameter values in equilibrium estimated as: $R_{1s} + R_{3e} = 8\ \mathrm{k\Omega}$, $R_{2s} = 140\ \mathrm{k\Omega}$, $C_{2s} = 3\mu\mathrm{F}$, $R_{4e} = 150\mathrm{k\Omega}$ and $C_{4e} = 180$ nF.

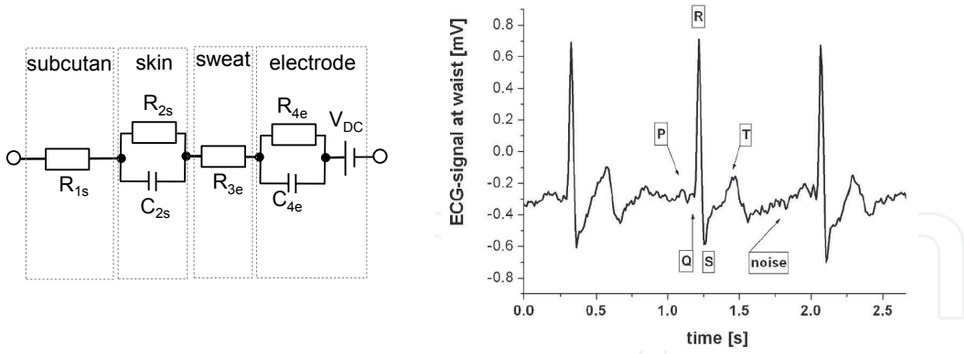

(a) A double-time-constant model of the skin-electrode interface.

(b) Sample ECG recording with dry electrodes in equilibrium.

Fig. 8. Figures showing (a) the equivalent electrical representation of the skin-electrode assumed by Mühlsteff et al and (b) a sample ECG recording (from (Mühlsteff & Such, 2004)).

An instrumentation amplifier having 10 MΩ input impedance was then used for recording the ECG shown in Fig. 8(b). The record clearly displays the QRS complex and the T wave. The P wave can also be identified despite its low amplitude. However, it can be observed that the baseline is not horizontal, especially immediately following abrupt voltage variations associated with the QRS complex and the T wave. Such effects can be attributed to low-frequency distortion similar to that reported by Tayler & Vincent (Tayler & Vincent, 1983). The authors have investigated the origin of the observed distortion by reproducing the low-frequency response of the dry-electrode design suggested Mühlsteff et al. Several different input capacitance values available in non-electrolytic form were used, ranging from 0.33 to 3.3 μF. Given $R_{in} = 10$ MΩ, the 3-dB point of the simulated high-pass filters varies between 0.05 and 0.005 Hz, and therefore meets AHA recommendations. This allows assessment of whether or not the low-frequency distortion suspected on the ECG recording of Fig. 8(b) might be caused by a degradation of the frequency response due to the presence of the double-time-constant skin-electrode interface. Results are presented in Fig. 9 and Table 2. Results from the simulated skin-electrode-amplifier network using the double-time-constant model indicate that for $R_{in} = 10$ MΩ, a cutoff frequency of about 0.03 Hz or lower is needed to fulfil both amplitude and phase requirements ($C_{in} \geq 0.47$ μF). It suggests that the presence of the modelled skin-electrode interface impedance has increased the effective 3-dB point of the skin-electrode-amplifier network. However, this increase alone cannot explain the level of distortion observed on the ECG of Fig. 8(b). Frequency response plots shown in Figs. 9(a) and 9(b) suggest that the amplitude and phase response would remain very close to that of a 0.05-Hz single-pole high-pass filter if C_{in} was equal to 0.33 μF.

Fig. 9(c) gives plots of the systems' response to a 3-mV pulse of 100-ms duration. As R_{in} remains constant, the offset following the input impulse is less than 0.1 mV for $C_{in} \geq 1$ μF, suggesting that in the presence of the skin-electrode impedance defined above, a lower 3-dB point of about 16 mHz is needed to meet the requirement of maximum undershoot. Fig. 9(d) is a graph of the recovery slope after the 300-mVs input impulse. The maximum slope of the response immediately after the impulse is about 1.6 mVs^{-1}, five times the allowed limit, and shows little variation when C_{in} is increased from 0.33 μF to 3.3 μF. In comparison, the recovery slope exhibited by a 0.05 Hz high-pass filter is not greater than 0.03 mVs^{-1}. Consequently, the

slope of the impulse response is not satisfactory for the range of input capacitances simulated. Excessively high recovery slope can therefore explain why the baseline of the ECG recording of Fig. 8(b) is not horizontal, immediately following abrupt voltage variations.
These results confirm that amplitude and phase requirements provide necessary conditions for the reproduction of low-frequency components of the ECG but they are not sufficient to prevent distortion and possible clinical misinterpretation of the waveform.

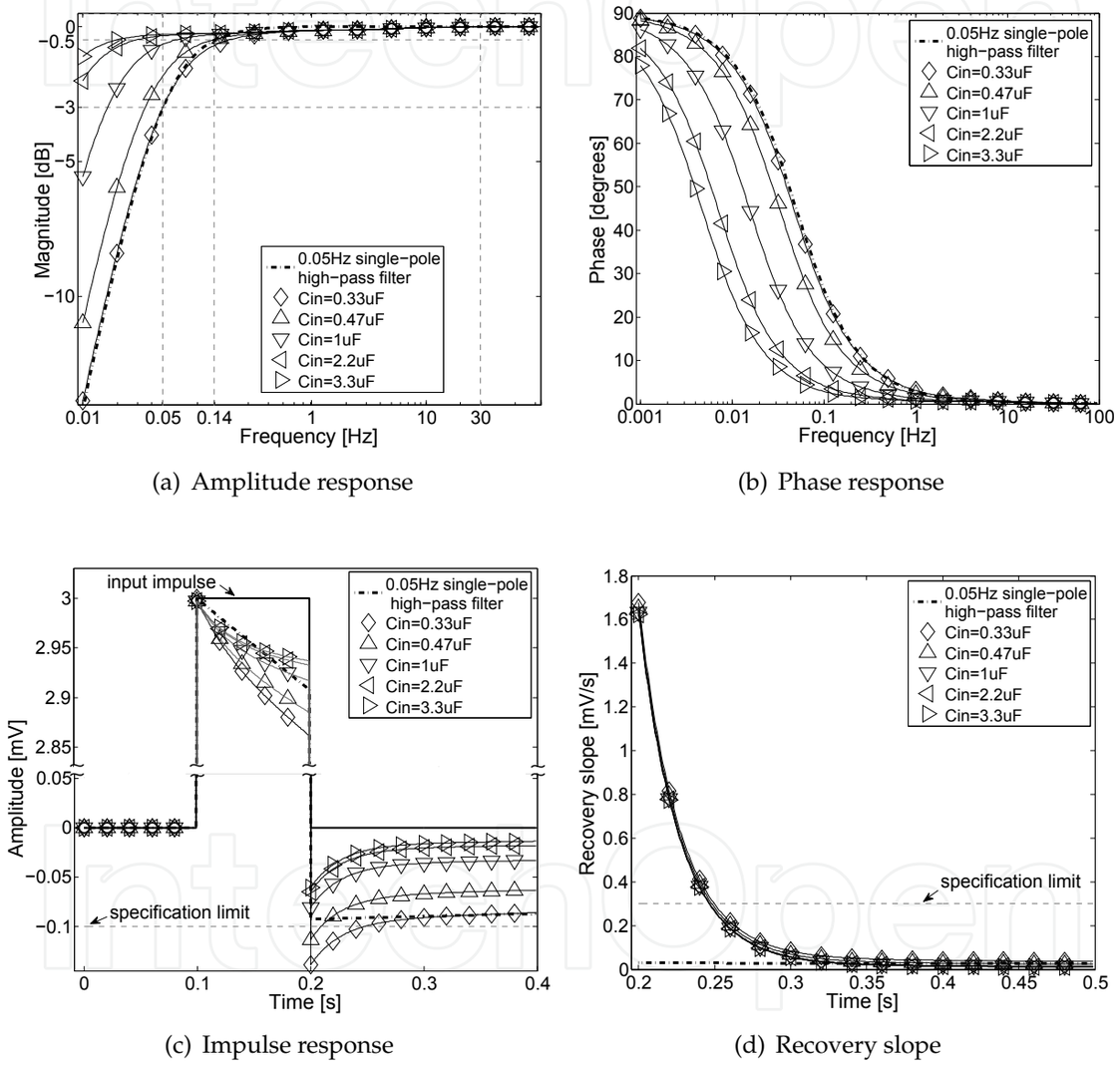

(a) Amplitude response

(b) Phase response

(c) Impulse response

(d) Recovery slope

Fig. 9. Plots of (a) the amplitude response, (b) phase response, (c) impulse response and (d) recovery slope of simulated transfer functions based on the design suggested by Mühlsteff et al. compared to that of a 0.05-Hz single-pole high-pass filter.

	max. magnitude 0.14-30 Hz [dB]	phase @ 0.5 Hz [°]	max. undershoot after impulse [mV]	max. slope [mVs^{-1}]
specification limit	-0.5	6	-0.1	0.3
0.5-Hz single-pole high-pass filter	-0.5	5.8	-0.093	0.03
C_{in}=0.33 μF	**−0.72**	5.9	**−0.14**	**1.68**
C_{in}=0.47 μF	-0.49	4.3	**−0.11**	**1.65**
C_{in}=1 μF	-0.29	2.3	-0.08	**1.63**
C_{in}=2.2 μF	-0.25	1.3	-0.07	**1.62**
C_{in}=3.3 μF	-0.25	1	-0.06	**1.62**

Table 2. Low-frequency performance of simulated transfer functions based on the design model by Mühlsteff et al. compared to that of a single-pole 0.05-Hz high-pass filter: $R_{in} = 10$ MΩ, $R_{1s} + R_{3e} = 8$ kΩ, $R_{2s} = 140$ kΩ, $C_{2s} = 3$ μF, $C_{4e} = 0.18$ μF. Bold case indicates that the requirement is not met.

3.3 Discussion

Simulation results have shown that the input impedance specification stated in international standards is not consistent with the accompanying low-frequency performance requirements. In addition, despite fulfilling both amplitude and phase criteria, some designs may fall short of meeting the impulse response requirements when the skin-electrode impedance is taken into account for dry-electrode recording. For the range of input capacitance values used, simulations based on the double-time-constant skin-electrode model indicate that the recovery slope is not significantly affected by a change of C_{in}. This can be explained by the presence of capacitive elements as small as 0.18 μF in the skin-electrode interface. The reactance of the electrode impedance is therefore considerably greater than that of C_{in} and dominates the reactance of the skin-electrode-amplifier network. It can therefore be concluded that:

1. Impulse response considerations must be included as an inherent part of the design strategy of new dry-electrode preamplifiers.
2. A complete characterisation of the skin-electrode interface is fundamental for the appropriate design of the amplifier front-end.
3. Meeting the impulse response specifications implies tighter requirements than compliance with the amplitude and phase criteria when the electrode impedance is taken into account.
4. The optimum values of R_{in} and C_{in} must be determined in relation to the parameter values of the skin-electrode interface so that all low-frequency requirements are simultaneously fulfilled.

4. New methods of characterisation of the skin-electrode interface

Previous studies have demonstrated that measurement of the dc skin-electrode impedance does not provide sufficient information. Because of the capacitive components, corresponding to the epidermal layer and the electrode's permittivity, ac measurement is needed to obtain an accurate estimate of the skin-electrode impedance (Zepeda-Carapia et al., 2005). The research group of which the authors are members has attempted to measure the resistive and capacitive properties of wet and dry electrodes using two experimental approaches,

namely frequency-domain based and time-domain based measurement. Several identification algorithms were also considered by the group: an asymptotic method requiring only five points extracted from the frequency response and curve fitting based on least squares error minimisation algorithms.

4.1 Instrumentation set-up

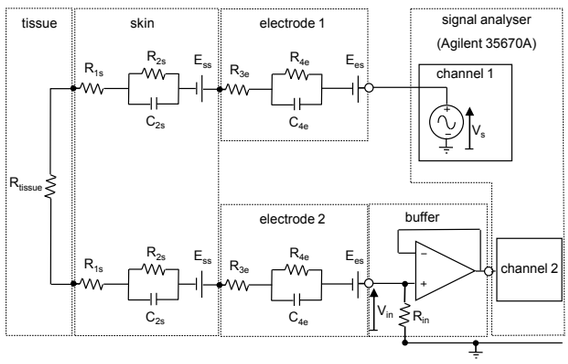

Fig. 10. Schematic representation of the measurement set-up assuming a double-time-constant model.

Impedance spectroscopy is generally the method applied to characterise the skin-electrode interface in the frequency range 0.05 Hz to 1 MHz (Burke & Gleeson, 2000; Chang et al., 2010; Gruetzmann et al., 2007; Ko et al., 1970; Mühlsteff & Such, 2004; Valverde et al., 2004; Zepeda-Carapia et al., 2005). The measured impedance is then fitted to an equivalent electrical model to identify the resistive and capacitive elements of the interface. Fig. 10 shows the instrumentation set-up considered by the authors for measuring the frequency response of the skin-electrode interface which consists of a dual electrode configuration connected to a resistive load, R_{in}. One electrode is fed with a sinusoidal voltage from a signal analyser (Agilent 35670A) and connected to the body. A second electrode is used to detect the resulting signal from the skin and feeds it to the input of the analyser. The selected signal analyser can generate sinusoidal signals in the frequency range 15 mHz to 51 kHz.

4.2 The proposed identification method

Fig. 11 shows the asymptotic bode diagram and the simulated frequency response of the interface based on the parameter values reported by Mühlsteff et al. ($R_{1s} + R_{3e} = 8$ kΩ, $R_{2s} = 140$ kΩ, $C_{2s} = 3$ μF, $R_{4e} = 150$ kΩ , $C_{4e} = 180$ nF and $R_{in} = 10$ MΩ) (Mühlsteff & Such, 2004). For the model provided, the phase response exhibits three local extrema at $f_1 = 0.45$ Hz, $f_2 = 1.40$ Hz and $f_3 = 5.26$ Hz. The authors have developed a novel method for the characterisation of the interface that relies upon knowledge of these three frequencies, and the attenuation introduced by the interface at low and high frequency. Taking $\tau_{2s} = R_{2s}C_{2s}$ and $\tau_{4e} = R_{4e}C_{4e}$, the phase measured at the amplifier input and its first derivative with respect to the angular frequency ω are given in eqs. (4) and (5) as:

$$\varphi(\omega) = tan^{-1}\left(\frac{\omega\frac{R_{2s}\tau_{2s}+R_{4e}\tau_{4e}}{R_{in}+2(R_{1s}+R_{2s}+R_{3e}+R_{4e})} + \omega^3\tau_{2s}\tau_{4e}\frac{R_{4e}\tau_2+R_{2s}\tau_{4e}}{R_{in}+2(R_{1s}+R_{2s}+R_{3e}+R_{4e})}}{1+\omega^2\frac{\tau_{2s}^2[R_{in}+2(R_{1s}+R_{3e}+R_{4e})]+\tau_{4e}^2[R_{in}+2(R_{1s}+R_{3e}+R_{4e})]}{R_{in}+2(R_{1s}+R_{2s}+R_{3e}+R_{4e})}+\omega^4\frac{[R_{in}+2(R_{1s}+R_{3e})]\tau_{2s}^2\tau_{4e}^2}{R_{in}+2(R_{1s}+R_{2s}+R_{3e}+R_{4e})}}\right) \quad (4)$$

$$\frac{d\varphi(\omega)}{d\omega} = \frac{1+a_1\omega^2+a_2\omega^4+a_3\omega^6}{\left[1+\left[\frac{\tau_{2s}^2[R_{in}+2(R_{1s}+R_{3e}+R_{4e})]+\tau_{4e}^2[R_{in}+2(R_{1s}+R_{2s}+R_{3e})]}{R_{in}+2(R_{1s}+R_{2s}+R_{3e}+R_{4e})}\right]\omega^2+\left[\frac{R_{in}+2(R_{1s}+R_{3e})}{R_{in}+2(R_{1s}+R_{2s}+R_{3e}+R_{4e})}\tau_{2s}^2\tau_{4e}^2\right]\omega^4\right]^2 + \left[\left[\frac{2R_{2s}\tau_{2s}+2R_{4e}\tau_{4e}}{R_{in}+2(R_{1s}+R_{2s}+R_{3e}+R_{4e})}\right]\omega+\left[\frac{2R_{2s}\tau_{4e}+2R_{4e}\tau_{2s}}{R_{in}+2(R_{1s}+R_{2s}+R_{3e}+R_{4e})}\tau_{2s}\tau_{4e}\right]\omega^3\right]^2} \quad (5)$$

where

$$a_1 = \frac{3\left(R_{4e}\tau_{2s}+R_{2s}\tau_{4e}\right)\tau_{2s}\tau_{4e}}{R_{2s}\tau_{2s}+R_{4e}\tau_{4e}} - \frac{\tau_{2s}^2\left[R_{in}+2\left(R_{1s}+R_{3e}+R_{4e}\right)\right]+\tau_{4e}^2\left[R_{in}+2\left(R_{1s}+R_{2s}+R_{4e}\right)\right]}{R_{in}+2\left(R_{1s}+R_{2s}+R_{3e}+R_{4e}\right)} \quad (6)$$

$$a_2 = \frac{\tau_{2s}\tau_{4e}\left[\tau_{2s}^2\left[R_{in}+2\left(R_{1s}+R_{3e}+R_{4e}\right)\right]+\tau_{4e}^2\left[R_{in}+2\left(R_{1s}+R_{2s}+R_{3e}\right)\right]\right]\left(\tau_{2s}R_{4e}+\tau_{4e}R_{2s}\right)}{\left[R_{in}+2\left(R_{1s}+R_{2s}+R_{3e}+R_{4e}\right)\right]\left(R_{2s}\tau_{2s}+R_{4e}\tau_{4e}\right)} - \frac{3\tau_{2s}^2\tau_{4e}^2\left[R_{in}+2\left(R_{1s}+R_{3e}\right)\right]}{R_{in}+2\left(R_{1s}+R_{2s}+R_{3e}+R_{4e}\right)} \quad (7)$$

$$a_3 = -\frac{\tau_{2s}^3\tau_{4e}^3\left[R_{in}+2\left(R_{1s}+R_{3e}+R_{4e}\right)\right]\left(R_{4e}\tau_{2s}+R_{2s}\tau_{4e}\right)}{\left[R_{in}+2\left(R_{1s}+R_{2s}+R_{3e}+R_{4e}\right)\right]\left(R_{2s}\tau_{2s}+R_{4e}\tau_{4e}\right)} \quad (8)$$

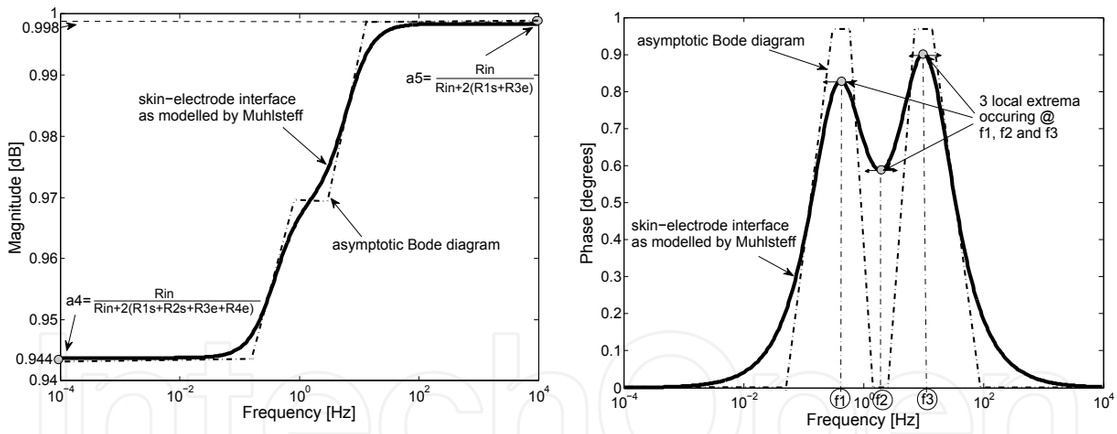

(a) Amplitude response (b) Phase response

Fig. 11. Plots of (a) the magnitude response and (b) the phase response of the skin-electrode interface as defined by Mühlsteff et al. for $R_{in} = 10\ \mathrm{M}\Omega$.

The three frequencies f_1, f_2 and f_3 identified in Fig. 11(b) are associated with three angular frequencies $\omega_1 = 2\pi f_1$, $\omega_2 = 2\pi f_2$ and $\omega_3 = 2\pi f_3$ that correspond to the positive and real solutions of $\frac{d\varphi(\omega)}{d\omega} = 0$. The following system of equations is then obtained:

$$\begin{cases} 1+a_1\omega_1^2+a_2\omega_1^4+a_3\omega_1^6 = 0 & (9) \\ 1+a_1\omega_2^2+a_2\omega_2^4+a_3\omega_2^6 = 0 & (10) \\ 1+a_1\omega_3^2+a_2\omega_3^4+a_3\omega_3^6 = 0 & (11) \end{cases}$$

It can be shown that the system defined in eqs. (9) to (11) can be rearranged to give the coefficients as:

$$\begin{cases} a_1 = -\dfrac{1}{\omega_1^2} - \dfrac{1}{\omega_2^2} - \dfrac{1}{\omega_3^2} & (12) \\ a_2 = \dfrac{\omega_1^2 + \omega_2^2 + \omega_3^2}{\omega_1^2 \omega_2^2 \omega_3^2} & (13) \\ a_3 = -\dfrac{1}{\omega_1^2 \omega_2^2 \omega_3^2} & (14) \end{cases}$$

In addition, the magnitude response shown in Fig. 11(a) exhibits two asymptotes at low and high frequency corresponding to:

$$a_4 = \lim_{\omega \to 0} \left| \frac{V_{in}(\omega)}{V_s(\omega)} \right| = \frac{R_{in}}{R_{in} + 2\left(R_{1s} + R_{2s} + R_{3e} + R_{4e}\right)} \tag{15}$$

and

$$a_5 = \lim_{\omega \to \infty} \left| \frac{V_{in}(\omega)}{V_s(\omega)} \right| = \frac{R_{in}}{R_{in} + 2\left(R_{1s} + R_{3e}\right)} \tag{16}$$

It can be noted that the magnitude response reaches more than 99.99% of its asymptotic values at 15 mHz and 1 kHz, giving good estimates of a_4 and a_5. The coefficients defined in eqs. (12) to (16) provide sufficient information for the identification of $q = \tau_{2s}\tau_{4e}$ as the positive and real solution of the following polynomial equation:

$$-\frac{3a_3^2 a_5^2}{a_4^2} - \frac{a_1 a_3 a_5}{a_4^2} q^2 + \frac{a_2}{a_4} q^4 + \frac{3}{a_5} q^6 = 0 \tag{17}$$

After solving eq. (17), the time constants are obtained from the positive solutions of the following equation:

$$1 + \frac{\left(a_1 a_4 q^2 + 3a_3 a_5\right)\left(a_3 a_5 - a_4 q^3\right) a_5 - \left(a_4 - a_5\right) q^3 \left(a_4 q^3 + a_3 a_5\right) a_4}{a_4 \left(a_3 a_5^2 - a_4^2 q^3\right) q^4} \tau^2 + \frac{1}{q^2} \tau^4 = 0 \tag{18}$$

Two valid solutions are then available for τ. In previous literature the skin contribution is considered to be dominant, therefore the larger of the two solutions can be allocated to τ_{2s}, the second one being τ_{4e}. Eqs. (12) to (18) are then utilised to determine the model parameters as:

$$R_{4e} = \frac{R_{in}}{2} \frac{\left(a_5 - a_4\right)\left(a_4 q^4 + a_5 a_3 \tau_{2s}^2\right)}{\left(a_3 a_5 - a_4 q^3\right) a_4 a_5 \left(\tau_{2s}^2 - q\right)} \tag{19}$$

$$R_{2s} = \frac{R_{in}}{2} \frac{\left(a_5 - a_4\right)}{a_4 a_5} - R_{4e} \tag{20}$$

$$C_{2s} = \frac{\tau_{2s}}{R_{2s}} \tag{21}$$

$$C_{4e} = \frac{q}{\tau_{2s} R_{4e}} \tag{22}$$

$$R_{1s} + R_{3e} = \frac{R_{in}}{2} \frac{(1 - a_5)}{a_5} \tag{23}$$

Only solutions that are real and positive are relevant for the purpose of parameter identification. For example, the five reference points indicated in the bode plot of Fig. 11 suggest the following coefficient values:

$$a_1 = -0.14 \mathrm{s}^2 \mathrm{rad}^{-2} \tag{24}$$

$$a_2 = 1.7 \mathrm{s}^2 \mathrm{rad}^{-2} \tag{25}$$

$$a_3 = -1.48 \mathrm{s}^2 \mathrm{rad}^{-2} \tag{26}$$

$$a_4 = 0.998 \tag{27}$$

$$a_5 = 0.944 \tag{28}$$

Applying theses values to eq. (17) yields:

$$-7.78 \text{ x } 10^{-12} - 2.30 \text{ x } 10^{-7} q^2 + 1.8 \text{ x } 10^{-3} q^4 + 3q^6 = 0 \tag{29}$$

Eq. (29) has a unique positive real solution at $q = \tau_{2s}\tau_{4e} = 0.0114$ s^2. This value is then inserted into eq. (18) to solve the following equation:

$$1 - 1.39 \text{ x } 10^3 \tau^2 + 7.71 \text{ x } 10^3 \tau^4 = 0 \tag{30}$$

The two positive solutions are: $\tau_{2s} = 0.423$ s and $\tau_{4e} = 0.027$ s. Taking $R_{in} = 10$ MΩ, the model parameters can then be deduced from eqs. (19) to (23) as:

$$R_{4e} \simeq 148 \text{ kΩ}, R_{2s} \simeq 139 \text{ kΩ}, C_{2s} \simeq 3 \text{ μF}, C_{4e} \simeq 182 \text{ nF and } R_{1s} + R_{3e} \simeq 10 \text{ kΩ}.$$

The small discrepancy observed between the estimated values and the simulated parameters is due to floating point approximation error in solving eqs. (17) and (18) and the limited precision with which a_4 and a_5 can be measured. The resolution method is described in more detail by the authors in (Assambo et al., 2006).

4.3 Measurement results

A hardware model of the skin-electrode interface was constructed using actual resistors and capacitors, based on the model provided by Mühlsteff et al. to assess the ability of the signal analyser to reproduce the simulated results shown in Fig. 11. A pair of 3.3-μF and 220-nF multi-layer ceramic capacitors simulated the effects of C_{2s} and C_{4e}, respectively, the original capacitance values (3 μF and 180 nF) being unavailable. Fig. 12 compares the measurement of magnitude and phase to that obtained as a result of the new identification method. Raw measurement data are filtered to remove measurement noise and to facilitate the detection of the two peaks and the trough in the phase response. The frequency of the three local extrema in the phase response and the two extremum values in the magnitude response allow the five

coefficients to be estimated and and the frequency response of the network to be simulated. A theoretical curve is included to assess the precision of the measurement and the accuracy of the fitted model.

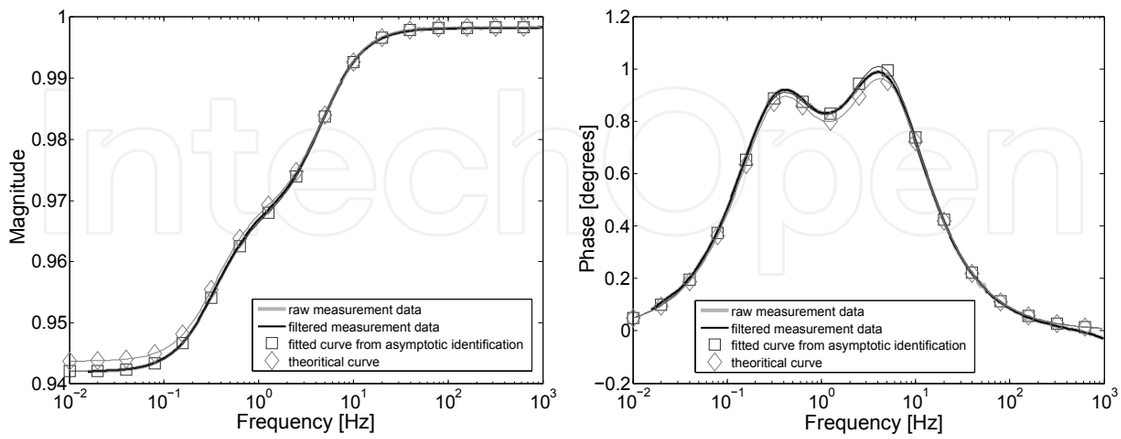

(a) Amplitude response (b) Phase response

Fig. 12. Comparison between the measured data ((a) magnitude and (b) phase) and data obtained as a result of the novel identification procedure for a constructed hardware model defined in Table 3.

The accuracy of the method can be appreciated from the results shown in Table 3, which suggest that if the skin-electrode interface in equilibrium behaves in a similar way as that measured by Mühlsteff et al., the proposed method would then provide a fast and accurate identification tool.

	actual component value	estimated value	% error
$R_{1s} + R_{3e}$ [kΩ]	8.20	8.47	+3.3 %
R_{2s} [kΩ]	140.00	141.21	+0.9%
R_{4e} [kΩ]	150.45	157.99	+5.1 %
C_{2s} [μF]	3.340	3.395	+1.6%
C_{4e} [μF]	0.219	0.218	-0.4 %

Table 3. Accuracy of the new identification method assessed from a constructed hardware model.

Fig. 13 shows measurements obtained in vivo with wet and dry electrodes which are significantly different than the results obtained with the hardware model.
It was observed that very often the phase response did not display two distinct peaks but only a single peak as shown in Fig. 13(a). This means that the polynomial $p(\omega) = 1 + a_1\omega^2 + a_2\omega^4 + a_3\omega^6$ has one real and positive root (ω_i), one real and negative root ($-\omega_i$) and four complex conjugate roots (ω_j, ω_j^*, $-\omega_j$ and $-\omega_j^*$). Similar results have been obtained from simulation when the time constant τ_{2s} and τ_{4e} differ by less than one order of magnitude, as shown in Fig. 14.

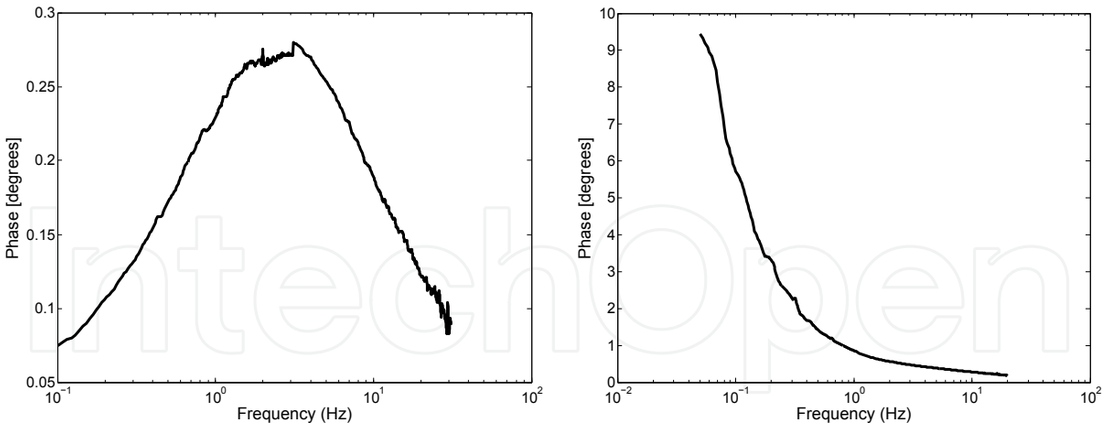

(a) wet electrodes (Wandy, E-50mm Hydrogel). (b) dry electrodes (Wandy, E-45).

Fig. 13. Typical phase response measurements obtained in vivo from (a) wet electrodes and (b) dry electrodes on the same subject.

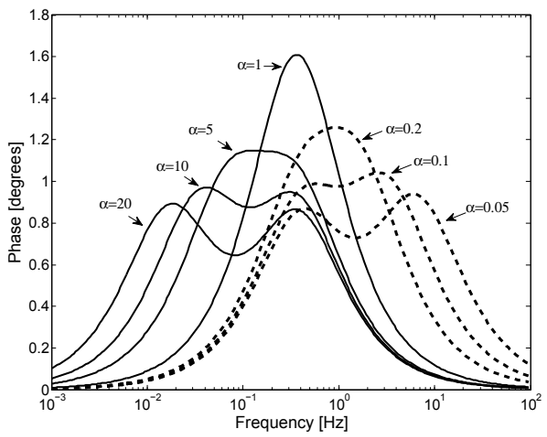

Fig. 14. Plot of the phase against frequency for different values of the ratio $\alpha = \frac{\tau_{2s}}{\tau_{4e}}$ when $R_{in} = 10$ MΩ, $R_{1s} + R_{3e} = 8$ kΩ, $R_{2s} = 140$ kΩ and $R_{4e} = 150$ kΩ.

4.4 Alternative approaches

Alternative approaches have been investigated to solve the parameter estimation problem in situations where the phase response does not display the expected double-peak behaviour. Dozio and Baba considered different fitting algorithms and measurement set-ups and concluded that time-domain measurements combined with least squares error minimisation were the most appropriate (Assambo et al., 2006; Baba & Burke, 2008; Dozio et al., 2007).

4.4.1 Fitting magnitude and phase

Dozio et al. first developed a least squares error minimisation program for fitting both the magnitude and phase response (Assambo et al., 2006). The algorithm successfully converged when applied to a pair of adhesive electrodes (Wandy, E-50mm Hydrogel) placed on the lower abdomen and returned the the following model parameters:

$$R_{1s} + R_{3e} = 3.6\ \text{k}\Omega,\ R_{2s} = 35.2\ \text{k}\Omega,\ C_{2s} = 0.9\ \mu\text{F},\ R_{4e} = 29.5\ \text{k}\Omega,\ C_{4e} = 5.8\ \mu\text{F}.$$

The experiment also confirmed that a simple 3-parameter model is not suitable for describing the skin-electrode impedance. The curve fitting algorithm did not however converge in the case of dry, pasteless electrodes (WANDY, W-45) for which the phase response exhibited no peak in the frequency range 0.05 to 30 Hz, as shown in Fig. 13(b). This was thought to be because the peak existed at a frequency below the minimum range of the analyser.

4.4.2 Time-based measurement

Frequency-based measurements have been unsuccessful when applied to dry electrodes since the characteristic frequencies are too low to allow reliable steady state measurement. To overcome this limitation time-based measurements have been developed. Baba et al. implemented a novel measurement technique that relies upon the time response of the skin-electrode interface to a current source (Assambo et al., 2006; Baba & Burke, 2008; Dozio et al., 2007). A constant current is fed through the body while measuring the skin-electrode impedance and a high-frequency sine wave input current is used to determine $R_{1s} + R_{3e}$. The knowledge of $R_{1s} + R_{3e}$ reduces the complexity of the fitting procedure to only four parameters and improves the accuracy of the results. Measurements were taken on seven subjects, using seven different types of dry electrodes, under variable conditions of contact pressure, electrode settling time and current level. Dozio developed a curve fitting program for the time-based data acquired. The time-domain measurement procedure and the results obtained are discussed in detail in (Baba & Burke, 2008).

Table 4 gives a summary of values for each component, measured across all subjects, electrodes, locations and contact pressures as published by Baba & Burke (Baba & Burke, 2008). The identification of the skin-electrode interface model parameters from two hundred and sixty eight measurements returned values of resistance ranging from 640 Ω to 2.54 MΩ and of capacitance ranging from 0.01 μF to 432.35 μF, while values of the time constants $\tau_{2s} = C_{2s}R_{2s}$ and $\tau_{4e} = C_{4e}R_{4e}$ varied from 0.02 s to 31.29 s. It was also discovered that there were substantial differences in the component values and the time constants between the rise and the fall phases in the step response of the skin-electrode interface. Worst-case parameter values obtained can now be used in the design of the input differential amplifier in ECG recording equipment to prevent low-frequency distortion of the ECG signal.

	Current rise phase		Current fall phase	
	min.	max.	min.	max.
$R_{1s} + R_{3e}$ [kΩ]	0.64	12	0.64	12
R_{2s} [kΩ]	4.94	1760.24	23.87	2540.93
R_{4e} [kΩ]	23.26	1840.52	84.78	1380.00
C_{2s} [μF]	0.01	21.51	0.04	21.88
C_{4e} [μF]	0.10	432.35	0.69	65.15
$R_{1s} + R_{2s} + R_{3e} + R_{4e}$ [kΩ]	161.24	3616.83	125.82	3326.10
τ_{2s} [s]	0.02	1.84	0.06	1.17
τ_{4e} [s]	0.18	31.29	0.77	7.19

Table 4. Summary of dry electrode parameter values published by Baba & Burke from 268 measurements (Baba & Burke, 2008).

5. New amplifier input impedance requirements for dry-electrode ECG recording

As seen in previous sections, the front-end amplifier plays a crucial role in the ability of the ECG recorder to preserve the low-frequency components of the signal. The low-frequency performance achieved by the amplifier in the presence of the electrode impedance is principally determined by the magnitude of the input impedance of the recording system. Fig. 15 shows the equivalent impedance seen at the amplifier input when skin-electrode interface, current limiting resistor (R_1) and the dc-blocking capacitors (C_{in}) are taken into account.

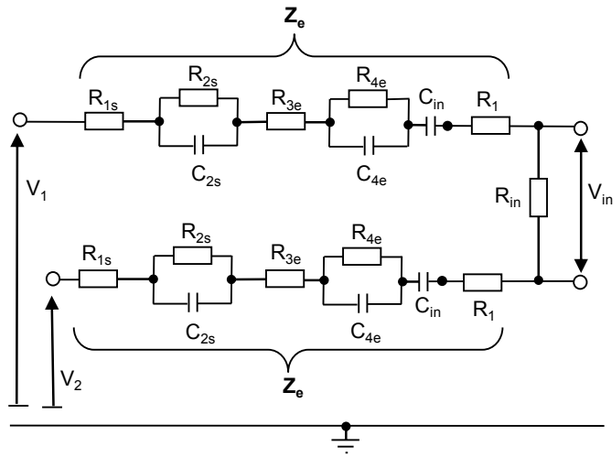

Fig. 15. Schematic representation of the equivalent impedance seen at the amplifier input.

The transfer function of the skin-electrode-amplifier network in this configuration is defined as follows:

$$H_d(s) = \frac{V_{in}(s)}{V_1(s) - V_2(s)} = R_{in}\frac{C_{in}}{2}\left[\frac{\tau_{2s}\tau_{4e}s^3 + (\tau_{2s} + \tau_{4e})\,s^2 + s}{d_3s^3 + d_2s^2 + d_1s + 1}\right] \tag{31}$$

where:

$$d_1 = [R_{in} + 2\,(R_1 + R_{1s} + R_{2s} + R_{3e} + R_{4e})]\,\frac{C_{in}}{2} + \tau_{2s} + \tau_{4e} \tag{32}$$

$$d_2 = [[R_{in} + 2\,(R_1 + R_{1s} + R_{3e})]\,(\tau_{2s} + \tau_{4e}) + 2R_{2s}\tau_{4e} + 2R_{4e}\tau_{2s}]\,\frac{C_{in}}{2} + \tau_{2s}\tau_{4e} \tag{33}$$

$$d_3 = [R_{in} + 2\,(R_1 + R_{1s} + R_{3e})]\,\frac{C_{in}}{2}\tau_{2s}\tau_{4e} \tag{34}$$

In the following sections, the authors establish new input impedance requirements for use in dry-electrode ECG recording.

5.1 Frequency response criteria

5.1.1 Amplitude response

The equivalent skin-electrode impedance, shown in Fig. 15, is responsible for a reduction in the signal amplitude before reaching the amplifier input. Minimum attenuation is obtained at high frequencies for which the impedance of capacitive elements in the electrode impedance tends toward zero, ensuring:

$$|H_d(\omega)| < \frac{R_{in}}{R_{in} + 2\,(R_1 + R_{1s} + R_{3e})} < 1 \tag{35}$$

At low frequencies, the source impedance is given by:

$$Z_e(\omega) = R_{1s} + R_{3s} + \frac{R_{2s}}{1 + j\omega R_{2s}C_{2s}} + \frac{R_{4e}}{1 + j\omega R_{4e}C_{4e}} + \frac{1}{j\omega C_1} + R_1 \tag{36}$$

The AHA recommends a maximum attenuation of 0.5 dB (or 6%) at 0.14 Hz, which establishes the requirement:

$$\frac{R_{in}}{|R_{in} + 2Z_e(\omega_{0.14})|} > 0.94 \tag{37}$$

where $\omega_{0.14} = 0.28\pi$.
It can be shown that the condition specified in eq. (37) implies the following relationship between R_{in} and the parameters of the skin-electrode interface:

$$\begin{aligned} R_{in}^2 \frac{1 - 0.94^2}{0.94^2} - 4R_{in}\left[R_1 + R_{1s} + R_{3e} + \frac{R_{2s}}{1 + \tau_{2s}^2\omega_{0.14}^2} + \frac{R_{4e}}{1 + \tau_{4e}^2\omega_{0.14}^2}\right] \\ - 4\left[R_1 + R_{1s} + R_{3e} + \frac{R_{2s}\tau_{2s}\omega_{0.14}}{1 + \tau_{2s}^2\omega_{0.14}^2} + \frac{R_{4e}\tau_{4e}\omega_{0.14}}{1 + \tau_{4e}^2\omega_{0.14}^2} + \frac{1}{\omega_{0.14}C_{in}}\right]^2 \\ - 4\left[R_1 + R_{1s} + R_{3e} + \frac{R_{2s}}{1 + \tau_{2s}^2\omega_{0.14}^2} + \frac{R_{4e}}{1 + \tau_{4e}^2\omega_{0.14}^2}\right]^2 > 0 \end{aligned} \tag{38}$$

The amplitude response criterion is then fulfilled for R_{in} selected as follows:

$$\begin{aligned} R_{in} > \frac{2 * 0.94^2}{1 - 0.94^2}\sqrt{\begin{array}{l}\left(R_1 + R_{1s} + R_{3e} + \frac{R_{2s}}{1+\tau_{2s}^2\omega_{0.14}^2} + \frac{R_{4e}}{1+\tau_{4e}^2\omega_{0.14}^2}\right)^2 \\ + \left(1 - 0.94^2\right)\left(R_1 + R_{1s} + R_{3e} + \frac{R_{2s}\tau_{2s}\omega_{0.14}}{1+\tau_{2s}^2\omega_{0.14}^2} + \frac{R_{4e}\tau_{4e}\omega_{0.14}}{1+\tau_{4e}^2\omega_{0.14}^2} + \frac{1}{\omega_{0.14}C_{in}}\right)^2\end{array}} \\ + \frac{2 * 0.94^2}{1 - 0.94^2}\left(R_1 + R_{1s} + R_{3e} + \frac{R_{2s}}{1 + \tau_{2s}^2\omega_{0.14}^2} + \frac{R_{4e}}{1 + \tau_{4e}^2\omega_{0.14}^2}\right) \end{aligned} \tag{39}$$

5.1.2 Phase response

The transfer function defined in eq. (31) can be rearranged so that real and imaginary parts are more easily identified:

$$H_d(\omega) = R_{in}\frac{C_{in}}{2}\left[\frac{\begin{array}{l}\left[\left(d_1 - \tau_{2s} - \tau_{4e}\right)\omega^2 + \left[d_2\left(\tau_{2s} + \tau_{4e}\right) - d_3\right]\omega^4 + d_1 d_3 \tau_{2s}\tau_{4e}\omega^6\right] \\ + j\left[\omega + \left(d_1\tau_{2s} + d_1\tau_{4e} - \tau_{2s}\tau_{4e}\right)\omega^3 + \left[d_2\tau_{2s}\tau_{4e} - d_3\left(\tau_{2s} + \tau_{4e}\right)\right]\omega^5\right]\end{array}}{\left(1 - d_2\omega^2\right)^2 + \left(d_1\omega - d_3\omega^3\right)^2}\right] \tag{40}$$

Replacing d_1, d_2 and d_3 by their expressions as given in eq.(32) to (34) yields the following:

$$H_d(\omega) = R_{in}\frac{C_{in}}{2}\omega \left[\begin{array}{l} R_T\frac{C_{in}}{2}\omega + \left[R_T\frac{C_{in}}{2}\left(\tau_{2s}^2+\tau_{4e}^2\right)+2\tau_{2s}\tau_{4e}\left(R_{2s}+R_{4e}\right)\frac{C_{in}}{2}\right]\omega^3 \\ +R_{13}\frac{C_{in}}{2}\tau_{2s}^2\tau_{4e}^2\omega^5 \\ +j[1+\left[2\left(R_{2s}\tau_{2s}+R_{4e}\tau_{4e}\right)\frac{C_{in}}{2}+\tau_{2s}^2+\tau_{4s}^2\right]\omega^2] \\ +j[\tau_{2s}\tau_{4e}\left[2\left(R_{2s}\tau_{4e}+R_{4e}\tau_{2s}\right)\frac{C_{in}}{2}+\tau_{2s}\tau_{4e}\right]\omega^4] \\ \hline \left[1-\left[\left[R_{13}\left(\tau_{2s}+\tau_{4e}\right)+2R_{2s}\tau_{4e}+2R_{4e}\tau_{2s}\right]\frac{C_{in}}{2}+\tau_{2s}\tau_{4e}\right]\omega^2\right]^2 \\ +\left[\left(R_T\frac{C_{in}}{2}+\tau_{2s}+\tau_{4e}\right)\omega-R_{13}\frac{C_{in}}{2}\tau_{2s}\tau_{4e}\omega^3\right]^2 \end{array} \right] \quad (41)$$

where

$$R_T = R_{in}+2\left(R_1+R_{1s}+R_{2s}+R_{3e}+R_{4e}\right) \quad (42)$$

and

$$R_{13} = R_{in}+2\left(R_1+R_{1s}+R_{3e}\right) \quad (43)$$

Since both imaginary and real parts of $H_d(\omega)$ are positive, an expression for the phase response can then be extracted from (41) as:

$$\varphi_d(\omega) = tan^{-1}\left(\frac{1+\left[\left(R_{2s}\tau_{2s}+R_{4e}\tau_{4e}\right)C_{in}+\tau_{2s}^2+\tau_{4s}^2\right]\omega^2+\tau_{2s}\tau_{4e}\left[\left(R_{2s}\tau_{4e}+R_{4e}\tau_{2s}\right)C_{in}+\tau_{2s}\tau_{4e}\right]\omega^4}{R_T\frac{C_{in}}{2}\omega+\left[R_T\frac{C_{in}}{2}\left(\tau_{2s}^2+\tau_{4e}^2\right)+\tau_{2s}\tau_{4e}\left(R_{2s}+R_{4e}\right)C_{in}\right]\omega^3+R_{13}\frac{C_{in}}{2}\tau_{2s}^2\tau_{4e}^2\omega^5}\right) \quad (44)$$

Eq. (44) indicates that:

$$0 < \varphi_d(\omega) < 90^\circ\ ,\ \forall\omega \in \Re^{+*} \quad (45)$$

The phase introduced by a single-pole high-pass filter having a cutoff frequency f_c is given by:

$$\Phi(\omega) = tan^{-1}\left(\frac{2\pi f_c}{\omega}\right) \quad (46)$$

The AHA recommends that the amplifier should introduce no more phase shift into the signal than that which would be introduced by a linear 0.05-Hz, single-pole filter. This condition is respected for $\varphi_d(\omega) < \Phi(\omega)$.
Both phase shifts belong to the interval $]0, \frac{\pi}{2}[$, in which the function *tan* is strictly increasing. The phase criterion is therefore equivalent to:

$$\frac{1+\left[\left(R_{2s}\tau_{2s}+R_{4e}\tau_{4e}\right)C_{in}+\tau_{2s}^2+\tau_{4s}^2\right]\omega^2+\tau_{2s}\tau_{4e}\left[\left(R_{2s}\tau_{4e}+R_{4e}\tau_{2s}\right)C_{in}+\tau_{2s}\tau_{4e}\right]\omega^4}{R_T\frac{C_{in}}{2}\omega+\left[R_T\frac{C_{in}}{2}\left(\tau_{2s}^2+\tau_{4e}^2\right)+\tau_{2s}\tau_{4e}\left(R_{2s}+R_{4e}\right)C_{in}\right]\omega^3+R_{13}\frac{C_{in}}{2}\tau_{2s}^2\tau_{4e}^2\omega^5} < \frac{2\pi f_c}{\omega} \quad (47)$$

Taking $\omega_c = 2\pi f_c$, the condition specified in eq. (47) is met for:

$$\left[\omega_c R_{13}\frac{C_{in}}{2}\tau_{2s}^2\tau_{4e}^2 - \tau_{2s}\tau_{4e}\left[\left(R_{2s}\tau_{4e} + R_{4e}\tau_{2s}\right)C_{in} + \tau_{2s}\tau_{4e}\right]\right]\omega^4$$
$$+\left[\omega_c\left[R_T\frac{C_{in}}{2}\left(\tau_{2s}^2+\tau_{4e}^2\right) + \tau_{2s}\tau_{4e}\left(R_{2s}+R_{4e}\right)C_{in}\right] - \left[\left(R_{2s}\tau_{2s}+R_{4e}\tau_{4e}\right)C_{in} + \tau_{2s}^2+\tau_{4s}^2\right]\right]\omega^2$$
$$+\omega_c R_T\frac{C_{in}}{2} - 1 > 0 \quad (48)$$

The polynomial function of eq. (48) is positive when two conditions are satisfied: (i) the coefficient of the highest power of ω is positive and (ii) there is no positive root. All roots must therefore be negative or complex. Both conditions are simultaneously met when:

$$\begin{cases} \omega_c R_{13}\frac{C_{in}}{2}\tau_{2s}^2\tau_{4e}^2 - \tau_{2s}\tau_{4e}\left[\left(R_{2s}\tau_{4e}+R_{4e}\tau_{2s}\right)C_{in}+\tau_{2s}\tau_{4e}\right] > 0 & (49) \\ \omega_c R_T\frac{C_{in}}{2} - 1 > 0 & (50) \end{cases}$$

Substituting $\tau_{2s} = R_{2s}C_{2s}$, $\tau_{4e} = R_{4e}C_{4e}$, $R_{13} = R_{in} + 2\left(R_1 + R_{1s} + R_{3e}\right)$ and $R_T = R_{13} + 2\left(R_{2s} + R_{4e}\right)$, eqs. (49) and (50) become:

$$\begin{cases} R_{in} > \frac{2}{\omega_c}\left(\frac{1}{C_{2s}}+\frac{1}{C_{4e}}+\frac{1}{C_{in}}\right) - 2\left(R_1+R_{1s}+R_{3e}\right) & (51) \\ R_{in} > \frac{2}{C_{in}\omega_c} - 2\left(R_1+R_{1s}+R_{2s}+R_{3e}+R_{4e}\right) & (52) \end{cases}$$

Eq. (52) establishes the phase criterion at low frequency, when the reactance of the capacitive effects in the skin-electrode interface tends towards infinity. At these frequencies C_{2s} and C_{4e} are equivalent to open switches making the skin-electrode impedance purely resistive. Phase shift is therefore solely introduced by the input capacitance C_{in}. This result is consistent with traditional design strategies which state that low-frequency distortion can be prevented if $R_{in}C_{in} > 1/\omega_c$, since other capacitive effects are neglected (Bergey et al., 1971; Valverde et al., 2004).

As frequency increases, the effects of C_{2s} and C_{4e} must be considered and eq. (51) ensures that the phase of the combined skin-electrode-amplifier network will not be greater than that introduced by a high-pass filter having a single pole at $f_c = \omega_c/2\pi$. Experience with insulated electrodes have shown that the effect of changing skin impedance can be minimised by making the coupling capacitance at least two orders of magnitude smaller than those of the skin. Coupling capacitance values ranging from 50 nF to 1 fF (f= 10^{-15}) have thus been used with buffer amplifiers having 10^8 to 10^{18} Ω input impedance (Ko et al., 1970; Prance et al., 2008; Taheri et al., 1994). Eq. (51) confirms that for $C_{in} << \{C_{2s}, C_{4e}\}$, the reactance of the skin-electrode interface can be neglected, and therefore selecting $R_{in}C_{in} > 1/\omega_c$ would prevent distortion. However, this approach involves the use of ultra-high input impedance amplifiers, whereas, the input impedance requirement can be relaxed if eq. (51) is applied instead.

With $f_c = 0.05$ Hz, the phase requirement is satisfied at all frequencies when the input impedance is chosen such that for the worst-case values of skin-electrode parameters:

$$R_{in} > \frac{20}{\pi}\left(\frac{1}{C_{2s}}+\frac{1}{C_{4e}}+\frac{1}{C_{in}}\right) \quad (53)$$

5.2 Impulse response requirements

In more recent years, the IEC have defined more precisely the low-frequency criteria for ECG signal reproduction in terms of the system impulse response. The response to a rectangular pulse $x(t)$ of amplitude V_m and duration T is limited to a maximum offset, ΔV_{max}, and a maximum slope, s_{max}. Fig. 16 shows in a generic form the impulse response requirement defined by international standards.

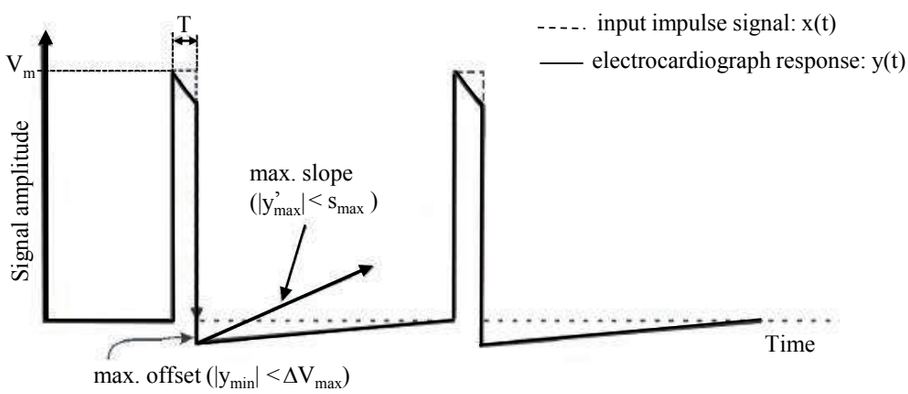

Fig. 16. Schematic illustrating the impulse response requirements.

The rectangular pulse $x(t)$ is ideally modelled using the Heaviside unit step function u as:

$$x(t) = V_m \left[u(t) - u(t-T)\right] \tag{54}$$

The Laplace transform of $x(t)$ is therefore given by:

$$X(s) = \frac{V_m}{s}\left(1 - e^{-Ts}\right) \tag{55}$$

Using the transfer function $H_d(s)$ defined in eq. (31), the frequency response $Y_d(s)$ of the skin-electrode-amplifier network to the pulse $X(s)$ is:

$$\begin{aligned} Y_d(s) = X(s)H_d(s) &= V_m\left(1 - e^{-Ts}\right) R_{in}\frac{C_{in}}{2}\left[\frac{\tau_{2s}\tau_{4e}s^2 + (\tau_{2s} + \tau_{4e})\,s + 1}{d_3 s^3 + d_2 s^2 + d_1 s + 1}\right] \\ &= V_m\left(1 - e^{-Ts}\right) R_{in}\frac{C_{in}}{2}\tau_{2s}\tau_{4e}\left[\frac{\left(s + \frac{1}{\tau_{2s}}\right)\left(s + \frac{1}{\tau_{4e}}\right)}{d_3\,(s-p_1)\,(s-p_2)\,(s-p_3)}\right] \end{aligned} \tag{56}$$

where p_0, p_1 and p_2 are the poles of $H_d(s)$, and d_1, d_2 and d_3 are defined in eqs. (32) to (34). Substituting d_3 by its expression allows $Y_d(s)$ to be simplified as follows:

$$Y_d(s) = \frac{R_{in}}{R_{13}} V_m\left(1 - e^{-Ts}\right)\left[\frac{\left(s + \frac{1}{\tau_{2s}}\right)\left(s + \frac{1}{\tau_{4e}}\right)}{(s-p_1)\,(s-p_2)\,(s-p_3)}\right] \tag{57}$$

with R_{13} given in eq. (43). The impulse response can then be expanded by partial fractions as:

$$Y_d(s) = \frac{R_{in}}{R_{13}} V_m\left(1 - e^{-Ts}\right)\left[\frac{A_0}{(s-p_0)} + \frac{A_1}{(s-p_1)} + \frac{A_2}{(s-p_2)}\right] \tag{58}$$

where the three coefficients A_0, A_1 and A_2 are functions of the parameters of the skin-electrode-amplifier network. Eqs. (56) and (58) imply:

$$Y_d(s)(s-p_0) = \frac{R_{in}}{R_{13}} V_m \left(1-e^{-Ts}\right) \left[A_0 + (s-p_0)\frac{A_1}{(s-p_1)} + (s-p_0)\frac{A_2}{(s-p_2)}\right]$$
$$= \frac{R_{in}}{R_{13}} V_m \left(1-e^{-Ts}\right) \left[\frac{\left(s+\frac{1}{\tau_{2s}}\right)\left(s+\frac{1}{\tau_{4e}}\right)}{(s-p_1)(s-p_2)}\right] \quad (59)$$

Taking $s = p_0$ yields:

$$A_0 = \frac{\left(p_0+\frac{1}{\tau_{2s}}\right)\left(p_0+\frac{1}{\tau_{4e}}\right)}{(p_0-p_1)(p_0-p_2)} \quad (60)$$

A similar approach leads to expressions for A_1 and A_2 as follows:

$$A_1 = \frac{\left(p_1+\frac{1}{\tau_{2s}}\right)\left(p_1+\frac{1}{\tau_{4e}}\right)}{(p_1-p_0)(p_1-p_2)} \quad (61)$$

$$A_2 = \frac{\left(p_2+\frac{1}{\tau_{2s}}\right)\left(p_2+\frac{1}{\tau_{4e}}\right)}{(p_2-p_0)(p_2-p_1)} \quad (62)$$

The inverse Laplace transform of $Y_d(s)$ gives the corresponding response in time $y_d(t)$ as:

$$y_d(t) = \frac{R_{in}}{R_{13}} V_m \left(A_0 e^{p_0 t} + A_1 e^{p_1 t} + A_2 e^{p_2 t}\right) u(t)$$
$$- \frac{R_{in}}{R_{13}} V_m \left(A_0 e^{p_0 (t-T)} + A_1 e^{p_1 (t-T)} + A_2 e^{p_2 (t-T)}\right) u(t-T) \quad (63)$$

If $x(t)$ is an ideal pulse, the amplitude of the response following the end of the impulse is given by:

$$y_d(t)|_{t>T} = -\frac{R_{in}}{R_{13}} V_m \sum_{k=0}^{2} \left[A_k (e^{-p_k T} - 1) e^{p_k t}\right] \quad (64)$$

The derivative of $y(t)$ at $t > T$ defines the slope of the impulse response following the impulse:

$$y_d'(t)\big|_{t>T} = \left.\frac{dy_d(t)}{dt}\right|_{t>T} = -\frac{R_{in}}{R_{13}} V_m \sum_{k=0}^{2} \left[p_k A_k (e^{-p_k T} - 1) e^{p_k t}\right] \quad (65)$$

The poles p_0, p_1 and p_2 are obtained by solving the polynomial $d_3 s^3 + d_2 s^2 + d_1 s + 1 = 0$. Computing the equation with *Mathematica* returns the following solutions:

$$p_0 = -\frac{d_2}{3d_3} - \frac{2^{1/3}\left(-d_2^2+3d_1d_3\right)}{3d_3\left[-2d_2^3+9d_1d_2d_3-27d_3^2+\sqrt{4\left(-d_2^2+3d_1d_3\right)^3+\left(-2d_2^3+9d_1d_2d_3-27d_3^2\right)^2}\right]^{1/3}}$$
$$+ \frac{\left[-2d_2^3+9d_1d_2d_3-27d_3^2+\sqrt{4\left(-d_2^2+3d_1d_3\right)^3+\left(-2d_2^3+9d_1d_2d_3-27d_3^2\right)^2}\right]^{1/3}}{32^{1/3}d_3} \quad (66)$$

$$p_1 = -\frac{d_2}{3d_3} - \frac{\left(1+j\sqrt{3}\right)\left(-d_2^2+3d_1d_3\right)}{32^{1/3}d_3\left[-2d_2^3+9d_1d_2d_3-27d_3^2+\sqrt{4\left(-d_2^2+3d_1d_3\right)^3+\left(-2d_2^3+9d_1d_2d_3-27d_3^2\right)^2}\right]^{1/3}} - \frac{\left(1-j\sqrt{3}\right)\left[-2d_2^3+9d_1d_2d_3-27d_3^2+\sqrt{4\left(-d_2^2+3d_1d_3\right)^3+\left(-2d_2^3+9d_1d_2d_3-27d_3^2\right)^2}\right]^{1/3}}{62^{1/3}d_3} \quad (67)$$

$$p_2 = -\frac{d_2}{3d_3} - \frac{\left(1-j\sqrt{3}\right)\left(-d_2^2+3d_1d_3\right)}{32^{1/3}d_3\left[-2d_2^3+9d_1d_2d_3-27d_3^2+\sqrt{4\left(-d_2^2+3d_1d_3\right)^3+\left(-2d_2^3+9d_1d_2d_3-27d_3^2\right)^2}\right]^{1/3}} - \frac{\left(1+j\sqrt{3}\right)\left[-2d_2^3+9d_1d_2d_3-27d_3^2+\sqrt{4\left(-d_2^2+3d_1d_3\right)^3+\left(-2d_2^3+9d_1d_2d_3-27d_3^2\right)^2}\right]^{1/3}}{62^{1/3}d_3} \quad (68)$$

The terms d_1, d_2 and d_3 may be substituted with their expressions given in eqs. (32) to (34) to evaluate p_0, p_1 and p_2. This would allow $y_d(t)$ and $y'_d(t)$ to be represented in terms of the parameters of the skin-electrode-amplifier network and the input impedance requirement to be identified. However, this method involves solving non-linear functions in the complex domain for which analytical solutions are not available. An alternative approach consists of implementing a numerical algorithm to find the minimum value of R_{in} for which the recording system meets the impulse response requirements. An algorithm was developed in *MATLAB* to test the maximum undershoot and recovery slope for a range of values of R_{in}.

5.3 Results

Data collected from two hundred and sixty eight measurements of the skin-electrode interface are analysed using the proposed methods. Measurements were taken on seven subjects, using seven different types of dry electrodes, under variable conditions of contact pressure, electrode settling time and current level. As for simulations referred to in Section 2.1, the input capacitance is initially set at $C_{in} = 0.33$ μF. The current limiting resistor was chosen as $R_1 = 100$ kΩ, as recommended in previous literature (Burke & Gleeson, 2000).

5.3.1 Amplitude and phase criteria

Fig. 17(a) shows the frequency response of the skin-electrode-amplifier network when the input impedance is selected following the amplitude response criterion defined in eq. (39). For all measurements, the minimum input impedance that fulfils the amplitude response recommendation varies from 21 MΩ to 115 MΩ. Fig. 17(b) gives the corresponding results when the front-end is designed according to the phase response requirement indicated in eq. (53). Meeting the phase criterion requires an input impedance between 21 MΩ and 750 MΩ.

5.3.2 Impulse response criteria

Results from the analysis of the impulse response for all measurements are presented in Fig. 17. A rectangular wave of amplitude 3 mV and duration 100 ms is used as input. The response is analysed over a 2 s period. Fig. 17(c) shows a plot of the maximum undershoot produced for a range of input impedance values between 10 MΩ and 10 GΩ. In Fig. 17(d), the maximum absolute values of the slope of the responses following the impulse are shown over the same range of input impedance values. With $C_{in} = 0.33$ μF, the required minimum input impedance varies between 20 MΩ and 2 GΩ.

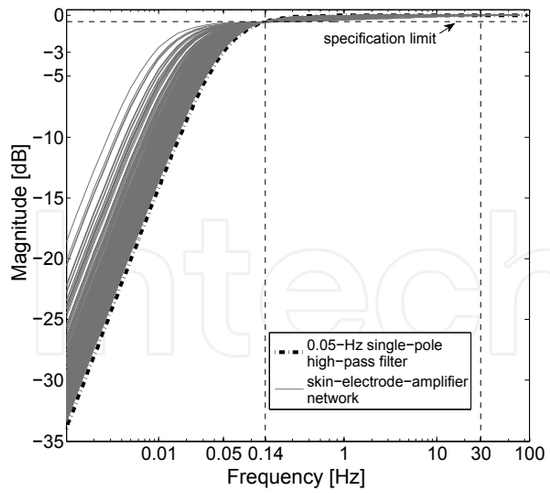

(a) Amplitude response with R_{in} as defined by eq. (39).

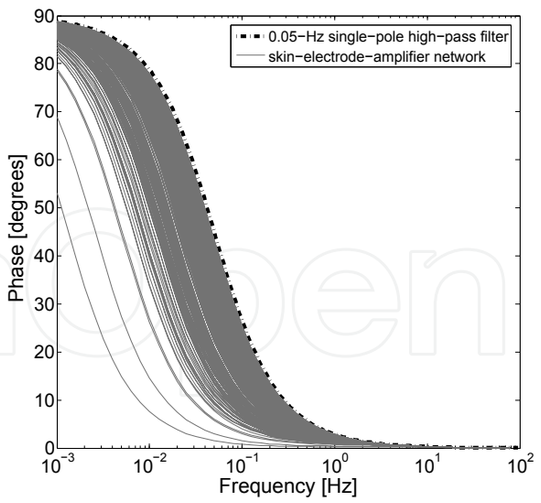

(b) Phase response with R_{in} as defined by eq. (53).

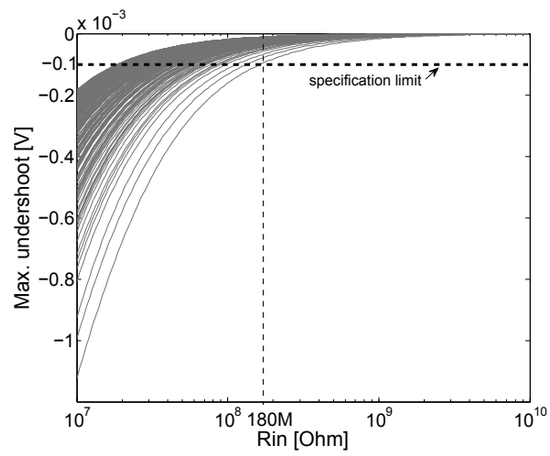

(c) Maximum undershoot vs. R_{in}.

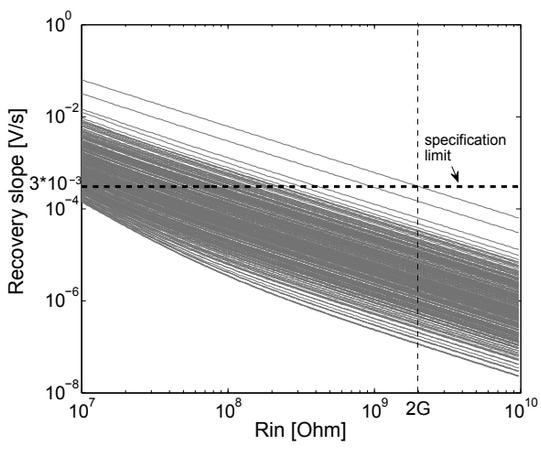

(d) Maximum slope absolute value vs. R_{in}.

Fig. 17. Plots of (a) the amplitude response, (b) phase response, (c) the maximum undershoot and (d) the maximum recovery slope for 268 measurements of skin-electrode interface impedance with $C_{in} = 0.33\mu$F and $R_1 = 100$ kΩ.

5.3.3 Influence of the coupling capacitance

Tables 5 and 6 compare the values of input impedance suggested by the frequency response and impulse response criteria. The values of R_{in} are given in both tables for a range of non-electrolytic capacitance values of C_{in} varying from 0.1 μF to 3.3 μF, available in multilayer ceramic forms. Table 5 gives the maximum values of input impedance suggested by all measurements. When one pair of outlying values is removed from the results, the requirements suggested by 99.2% of the data are shown in Table 6.

C_{in} [μF]	0.1	0.22	0.33	0.47	1	2.2	3.3
amplitude response: R_{in} [MΩ]	139	119	115	114	112	112	112
phase response: R_{in} [MΩ]	764	730	720	714	707	704	703
impulse response: R_{in} [MΩ]	2040	2040	2040	2040	2040	2040	2040

Table 5. Worst-case input impedance requirements as a function of the capacitance of the dc-blocking capacitor C_{in} for all 268 measurements.

C_{in} [μF]	0.1	0.22	0.33	0.47	1	2.2	3.3
amplitude response: R_{in} [MΩ]	120	96	91	89	87	86	86
phase response: R_{in} [MΩ]	236	201	192	185	180	175	174
impulse response: R_{in} [MΩ]	429	429	429	429	429	429	429

Table 6. Worst-case input impedance requirements as a function of the capacitance of the dc-blocking capacitor C_{in} for 99.2% of measurements.

Results for both tables indicate that the value of R_{in} levels out at around a value of $C_{in} = 1$ μF. As suggested by eq. (53), with increasing dc-blocking capacitance value, the parameters of the skin-electrode interface become the limiting factor. All results confirm that meeting the impulse response involves the highest values of input impedance, which are selected as the target design value. This is seen to be 2 GΩ, well above the IEC specification value of 10 MΩ. This again highlights the inappropriateness of this impedance specification for dry electrodes.

6. Conclusion

In this chapter, poor low-frequency response was shown to be a primary source of measurement error that jeopardises the ability of the ECG recording to provide reliable diagnostic clinical information. Despite being necessary to prevent base line wander, high-pass filtering can cause distortion in the ECG signal if implemented inadequately. A numerical tool was developed by the authors to assess the performance of passive high-pass filters up to fourth order against standards requirements. Simulation results have highlighted the lack of consistency between minimum input impedance requirement and low-frequency specifications in ECG standards. It was also demonstrated that the input impulse criteria imply more stringent requirements than the traditional amplitude and phase specifications. In particular, it was shown that recording systems for which the impulse response exhibits an unsatisfactory recovery slope may distort the ECG waveform despite providing acceptable amplitude and phase characteristics in the signal bandwidth. The need for new input impedance requirements that rely upon a complete characterisation of the skin-electrode interface was therefore identified.

Different approaches have been undertaken to model the skin-electrode interface. Experiences with self-adhesive electrodes confirmed that an early model which describes the interface as a single-time-constant RC network is inadequate. A model involving two time constants proves more accurate. Based on the latter model, an algorithm has been implemented to identify the parameters of any double-time-constant system the phase response of which displays a double-peak. Simulations returned highly accurate results when the two time constants forming the system are in a ratio of greater than 10 to 1. The method reaches its limits, however, when the time constants are close to each other and the difference in the phase of the two peaks in the response becomes too small to be accurately measured by the instruments available. Time-domain measurements were employed to obtain parameter values for dry,

pasteless electrodes. The fitting procedure converged when the rise and fall phases of the response were analysed separately, producing two estimates of the model parameters. The authors have then derived, using a combination of analytical and numerical methods, a set of input impedance requirements which ensure that performance specifications are met in dry-electrode recording. The minimum requirement for the input resistance of the amplifier is determined as 2 GΩ over a range of electrodes, measurement conditions and the value of dc-blocking capacitors used. However, 99.2% of measurements suggested that a value of R_{in} of 500 MΩ would meet requirements.

7. References

A.H.A. (1967). Recommendations for standardization of leads and of specifications for instruments in electrocardiography and vectorcardiography, *Circulation* 35: 583 – 602.

A.H.A. (1985). Aha special reports: Recommendations for standards of instrumentation and practice in the use of ambulatory electrocardiography, *Circulation* 71: 626A – 636A.

A.H.A. (1990). Recommendations for standardization and specifications in automated electrocardiography: bandwidth and digital signal processing. a report for health professionals by an ad hoc writing group of the committee on electrocardiography and cardiac electrophysiology of the council on clinical cardiology, american heart association, *Circulation* 81: 730 – 739.

Assambo, C., Baba, A., Dozio, R. & Burke, M. J. (2006). Parameter estimation of the skin-electrode interface model for high-impedance bio-electrodes, *WSEAS Transactions on Biology and Biomedicine* 3: 573 – 580.

Baba, A. & Burke, M. J. (2008). Electrical characterisation of dry electrodes for ecg recording, *Proceedings of the 12th WSEAS International Conference in Circuits Systems Communications and Computers*, Crete, Greece, pp. 591 – 596.

Bergey, G. E., Aquires, R. D. & Sipple, W. C. (1971). Electrocardiogram recording with pasteless electrodes, *IEEE Transactions on Bio-medical Engineering* BME-18: 206 – 211.

Berson, A. S., Galen, P., Adams, W. O., Adan, M., Berson, A. S., Briller, S. A., Daleo, S., Daly, D. L., Dobbins, J., Fink, M. N., Galen, P., Geselowitz, D., Gupte, P. M., Hernke, D., Klement, H., Milsap, J. P., Rutishauser, K., Smirles, W. J., Webster, J. G., Brown, D., Cangelosi, R., Charbonnier, F., Kutik, M. J. & Rowlandson, I. (2007). *ANSI/AAMI EC11:1991/(R)2001/(R)2007: Diagnostic electrocardiographic devices*.

Berson, S. & Pipberger, H. V. (1966). The low frequency response of electrocardiographs, a frequent source of recording errors, *Amererican Heart Journal* 71(6): 779 – 789.

Bruce, R. E., Moody, G., Bruce, R. E., Deedwania, P. C., Richard Gregg, P. M., Ho, C., Moody, G., Murray, W., Rutishauser, K., Sajadi, A., Sunderl, R. A., Young, B. J., Eloff, B. C., Marinello, S. A., Schneider, M. & Wang, J. (2007). *ANSI/AAMI EC38:2007: Medical electrical equipment - Part 2-47: Particular requirements for the safety, including essential performance, of ambulatory electrocardiographic systems*.

Burke, M. J. & Gleeson, D. T. (2000). A micropower dry-electrode ecg preamplifier, *IEEE Transactions on Biomedical Engineering* 47.

Chang, C.-L., Chang, C.-W., Huang, H.-Y., Hsu, C.-M., Huang, C.-H., Chiou, J.-C. & Luo, C.-H. (2010). A power-efficient bio-potential acquisition device with ds-mde sensors for long-term healthcare monitoring applications, *Sensors* 10: 4778 – 4793.

Dozio, R., Baba, A., Assambo, C. & Burke, M. J. (2007). Time based measurement of the impedance of the skin-electrode interface for dry electrode ecg recording, *Proceedings*

of the 29th Annual International Conference of the IEEE Engineering in Medicine and Biology Society, Lyon, France, pp. 5001 – 5004.

Fuhrhop, S., Lamparth, S., Kirst, M., Wagner, G. & Ottenbacher, J. (2009). Ambulant ecg recording with wet and dry electrodes: A direct comparison of two systems, *in* O. Dossel & W. C. Schlegel (eds), *IFMBE proceedings of the 2009 World Congress on Medical Physics and Biomedical Engineering*, Vol. 25 / V, Munich, Germany, pp. 305 – 307.

Gruetzmann, A., Hansen, S. & Müller, J. (2007). Novel dry electrodes for ecg monitoring, *Physiological Measurement* 28: 1375 – 1390.

I.E.C. (2001). *Medical electrical equipment Part 2-47: Particular requirements for the safety, including essential performance, of ambulatory electrocardiographic systems (IEC 60601-2-47:2001)*, 2nd edn.

I.E.C. (2005). *Medical electrical equipment Part 2-27: Particular requirements for the safety, including essential performance, of electrocardiographic monitoring equipment (IEC 60601-2-27:2005)*.

Ko, W. H., Neuman, M. R., Wolfson, R. N. & Yon, E. T. (1970). Insulated active electrodes, *IEEE Transactions on Industrial Electronics and Control Instrumentation* IECI-17: 195 – 198.

Lee, K.-H., Lee, J.-W., Jung, W.-C., Kim, K.-S., Jun, J.-H. & Kim, D.-J. (2006). Asymmetric skin-to-electrode impedance characterisation of concentric circular ring electrode for monitoring of electrical activity of the heart, *Proceedings of the SICE-ICASE International Joint Conference*, pp. 1135 – 1136.

Lynch, P., Dargie, H., Krickler, S. & Krickler, D. (1980). Objective assessment of anti-anginal treatment: A double blind comparison of propranolol, nifedipine, and their combination, *British Medical Journal* pp. 184 – 187.

Mühlsteff, J. & Such, O. (2004). Dry electrodes for monitoring of vital signs in functional textiles, *Proceedings of the 26th Annual International Conference of the IEEE EMBS*, San Francisco, CA, USA, pp. 2212 – 2215.

Prance, R. J., Beardsmore-Rst, S., Aydin, A., Harland, C. J. & Prance, H. (2008). Biological and medical applications of a new electric field sensor, *Proceedings of the ESA Annual Meeting on Electrostatics*.

Symanski, J. D. & Gettes, L. S. (1993). Drug effects on the electrocardiogram: a review of their clinical importance, *Drugs* 46: 219 – 248.

Taheri, B. A., Knight, R. T. & Smith, R. L. (1994). A dry electrode for eeg recording, *Electroencelography and Clinical Neurophysiology* 90: 376 – 383.

Tayler, D. & Vincent, R. (1983). Signal distortion in the electrocardiogram due to inadequate phase response, *IEEE Trans. Biomed. Eng.* 30(6): 352 – 356.

Valverde, E. R., Arini, P. D., Bertran, G. C., Biagetti, M. O. & Quinteiro, R. A. (2004). Effect of electrode impedance in improved buffer amplifier for bioelectric recordings, *Journal of Medical Engineering and Technology* 28: 217 – 222.

Wolfe, A. & Reinhold, H. (1974). *A Flexible, quick application ECG electrode system, in Biomedical Electrode Technology*, 1st edn, Academic Press, chapter 2, pp. 183 – 192.

Zepeda-Carapia, I., Marquez-espionaza, A. & Alvarado-Serrano, C. (2005). Measurement of the skin-electrode impedance for a 12-lead electrocardiogram, *Proceedings of the 2nd International Conference on Electronics Engineering and XI Conference on Electrical Engineering*, pp. 193 – 195.

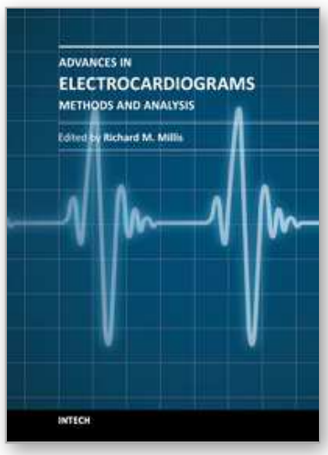

Advances in Electrocardiograms - Methods and Analysis
Edited by PhD. Richard Millis

ISBN 978-953-307-923-3
Hard cover, 390 pages
Publisher InTech
Published online 25, January, 2012
Published in print edition January, 2012

Electrocardiograms are one of the most widely used methods for evaluating the structure-function relationships of the heart in health and disease. This book is the first of two volumes which reviews recent advancements in electrocardiography. This volume lays the groundwork for understanding the technical aspects of these advancements. The five sections of this volume, Cardiac Anatomy, ECG Technique, ECG Features, Heart Rate Variability and ECG Data Management, provide comprehensive reviews of advancements in the technical and analytical methods for interpreting and evaluating electrocardiograms. This volume is complemented with anatomical diagrams, electrocardiogram recordings, flow diagrams and algorithms which demonstrate the most modern principles of electrocardiography. The chapters which form this volume describe how the technical impediments inherent to instrument-patient interfacing, recording and interpreting variations in electrocardiogram time intervals and morphologies, as well as electrocardiogram data sharing have been effectively overcome. The advent of novel detection, filtering and testing devices are described. Foremost, among these devices are innovative algorithms for automating the evaluation of electrocardiograms.

How to reference
In order to correctly reference this scholarly work, feel free to copy and paste the following:

Cédric Assambo and Martin J. Burke (2012). Low-Frequency Response and the Skin-Electrode Interface in Dry-Electrode Electrocardiography, Advances in Electrocardiograms - Methods and Analysis, PhD. Richard Millis (Ed.), ISBN: 978-953-307-923-3, InTech, Available from: http://www.intechopen.com/books/advances-in-electrocardiograms-methods-and-analysis/low-frequency-response-and-the-skin-electrode-interface-in-dry-electrode-electrocardiography

INTECH
open science | open minds

InTech Europe
University Campus STeP Ri
Slavka Krautzeka 83/A
51000 Rijeka, Croatia
Phone: +385 (51) 770 447
Fax: +385 (51) 686 166
www.intechopen.com

InTech China
Unit 405, Office Block, Hotel Equatorial Shanghai
No.65, Yan An Road (West), Shanghai, 200040, China
中国上海市延安西路65号上海国际贵都大饭店办公楼405单元
Phone: +86-21-62489820
Fax: +86-21-62489821

IntechOpen